

Aus der Universitätsklinik für Thorax-, Herz- und  
Gefäßchirurgie Tübingen  
Sektion Medizinische Werkstoffkunde und Technologie

**Osteoblast Responses to Different Surface  
Morphology and Roughness of 3D-printed PEEK  
Implants and Prosthesis**

Inaugural-Dissertation  
zur Erlangung des Doktorgrades  
der Zahnheilkunde

der Medizinischen Fakultät  
der Eberhard Karls Universität  
zu Tübingen

vorgelegt von  
Han, Xingting

2019

Dekan: Professor Dr. I. B. Autenrieth

1. Berichterstatter: Professor Dr. F. Rupp

2. Berichterstatter: Professor Dr. B. Koos

Tag der Disputation: 18.11.2019

## Contents

List of figures.....	III
List of tables.....	IV
List of Abbreviations.....	V
<b>1 Introduction.....</b>	<b>1</b>
<b>1.1 Bone restoration in oral-maxillofacial surgery .....</b>	<b>1</b>
<b>1.2 PEEK synthetic materials .....</b>	<b>2</b>
<b>1.3 Surface modification of PEEK.....</b>	<b>4</b>
1.3.1 Direct surface modification .....	4
1.3.2 Deposition Techniques .....	6
<b>1.4 PEEK composite .....</b>	<b>7</b>
<b>1.5 Additive manufacturing technology .....</b>	<b>7</b>
1.5.1 A brief review of additive manufacturing.....	7
1.5.2 The classification of AM technology.....	8
<b>1.6 Aim of the study.....</b>	<b>11</b>
<b>2 Materials and Methods.....</b>	<b>12</b>
<b>2.1 PEEK samples preparation.....</b>	<b>12</b>
<b>2.2 Surface modification of PEEK samples .....</b>	<b>14</b>
<b>2.3 Surface characterization .....</b>	<b>16</b>
2.3.1 Scanning electron microscopy (SEM) .....	16
2.3.2 Analysis of surface topography .....	17
2.3.3 Sessile-drop contact angle measurement .....	18
<b>2.4 Biological tests .....</b>	<b>19</b>
2.4.1 Osteoblast cell culture.....	19
2.4.2 Initial cell adhesion .....	20
2.4.3 Cell metabolic activity and proliferation assay.....	22
2.4.4 Surface coverage measurement.....	23
<b>2.5 Statistical analysis .....</b>	<b>23</b>
<b>3 Results.....</b>	<b>24</b>
<b>3.1 Surface characterization .....</b>	<b>24</b>
3.1.1 Surface morphology characterization .....	24
3.1.2 Surface roughness characterization .....	27
3.1.3 Contact angle measurement.....	34
<b>3.2 Biological tests .....</b>	<b>38</b>
3.2.1 Initial cell adhesion .....	38
3.2.2 Cell metabolic activity and proliferation .....	41
3.2.3 Sample surface coverage.....	43
<b>4 Discussion.....</b>	<b>48</b>
<b>5 Summary .....</b>	<b>55</b>

## Contents

---

<b>6</b>	<b>Zusammenfassung .....</b>	<b>57</b>
<b>7</b>	<b>References .....</b>	<b>59</b>
	<b>Declaration of Contribution .....</b>	<b>X</b>
	<b>Acknowledgment .....</b>	<b>XI</b>
	<b>Curriculum Vitae .....</b>	<b>XII</b>



**List of figures**

Figure 1 The clinical application of PEEK ..... 3

Figure 2 General strategies to improve PEEK's bioactivity ..... 4

Figure 3 The flow chart of the experiment ..... 12

Figure 4 Grit-blasting machine ..... 15

Figure 5 SEM device ..... 16

Figure 6 Surface topography measurement system (profilometer) ..... 17

Figure 7 Drop shape analysis device ..... 19

Figure 8 SEM images of different sample groups ..... 27

Figure 9 Reconstructed 3D surface topographies and Ra values ..... 34

Figure 10 Water contact angles ..... 37

Figure 11 Optical micrographs of initial cell adhesion ..... 40

Figure 12 Initial cell adhesion stained with crystal violet ..... 41

Figure 13 Cell metabolic activity and proliferation test ..... 43

Figure 14 Optical micrographs of surface coverage of SAOS-2 osteoblasts .... 46

Figure 15 Surface coverage stained with crystal violet ..... 47

Figure 16 Grit-blasted PEEK under different grit-blasting parameters ..... 49

Figure 17 LIVE/DEAD staining of L929 fibroblast..... 52

**List of tables**

Table 1 The elastic modulus of PEEK, Ti, ceramics, and human tissues..... 3

Table 2 Technical properties and the fabricating parameters of the printer. .... 13

Table 3 The material properties of PEEK filament..... 14

Table 4 Description of two-dimensional roughness parameters..... 18

Table 5 Roughness characterization. .... 28

Table 6 The OD values of cell proliferation test..... 42

## List of Abbreviations

**ABS:** acrylonitrile butadiene styrene

**MSC:** mesenchymal stem cell

**AM:** additive manufacturing

**ANAB:** accelerated neutral atom beam

**ANOVA:** analysis of variance

**CCK-8:** cell counting kit-8 assay

**CFR-PEEK:** carbon fiber reinforced PEEK

**CT:** computer tomography

**DI:** deionized

**DLC:** diamond-like carbon

**DSA:** drop shape analysis device

**FFF:** fused filament fabrication

**GCIB:** gas cluster ion beam

**HA:** hydroxyapatite

**MRI:** magnetic resonance imaging

**OD:** optical density

**PAEK:** polyaryletherketone

**PEEK:** polyetheretherketone

**PGA:** polyglycolide

**PHB:** polyhydroxybutyrate

**PLA:** polylactic acid

**PMMA:** polymethyl methacrylate

**Ra:** **average roughness** (arithmetical mean deviation of the assessed profile)

**Rku:** kurtosis of the assessed roughness profile

**RP:** rapid prototyping

**Rq:** root mean square deviation of the roughness profile

**Rsk:** skewness of the assessed roughness profile

**Rt:** total height of profile

**Rz:** maximum height of the roughness profile

**SEM:** scanning electron microscopy device

**SLA:** stereolithography

**SLS:** selective laser sintering

**TCPS:** tissue culture polystyrene

**TiO<sub>2</sub>:** titanium dioxide

**UV:** ultra violet

**β-TCP:** β-tricalcium phosphate

**3D:** three-dimensional

## 1 Introduction

### 1.1 Bone restoration in oral-maxillofacial surgery

Cranio-maxillofacial defects can be caused by tumors, traumas, infections or congenital deformities. The reconstruction of these defects is difficult for dental surgeries [1–3]. At present, there are four different bone graft materials to reconstruct those defects, autograft, allograft, xenograft, and synthetic materials [4–6].

Autograft (autogenous graft) bone is defined as tissue which is come from and applied in one body, which includes bone marrow, cancellous bone, cortical bone, and vascularized grafts [7]. The advantages of autogenous bone are simultaneously osteogenic, osteoinductive, and osteoconductive [6]. While the most important limitation of autogenous bone is the shape of the donor sites, like fibula, scapula and iliac crest [8,9] Besides, the bone inflammation after implantation also influences the clinical use of autogenous bone [10]. Allograft refers to bone tissue which is taken from one body and applied into another one (same species) [7]. Xenograft also means bone tissue is taken from one body into another, but in different species [7]. Immunological rejection and transmission of diseases (especially for viruses) hinders allografts and xenografts as an option for bone repair [11–14]. Synthetic materials greatly expand the available tools for bone grafting, which are currently considered as an optional treatment for the reconstruction of moderate to severe cranio-maxillofacial defects.

There are three main groups of synthetic materials, namely metals, ceramics, and polymers [4,15,16]. As a representative metal, titanium (Ti) is used widely in dentistry because of many advantages, like good corrosion resistance,

mechanical properties, and biocompatibility [17,18]. Unfortunately, stress-shielding and prosthetic loosening are the most important drawbacks of metal grafts due to the mismatch of the mechanical properties between metals and human bones. Furthermore, the existing metals might influence the X-ray examination, e.g., magnetic resonance imaging (MRI) and computer tomography (CT) images [19]. For ceramics, calcium phosphate, and metallic oxides are the most used. These materials have some similar advantages with Ti, like good mechanical properties and corrosion resistance [20]. However, the brittleness and Young's modulus of Ti and ceramics are much higher than human bone, which is unsuitable for bone replacement [21].

### **1.2 PEEK synthetic materials**

Because there are some disadvantages of metal and ceramics, in recent years, polymers are used widely in clinic and considered as an alternative material for them, e.g., polymethyl methacrylate (PMMA), polyglycolide (PGA), polylactide (PLA), and polyhydroxybutyrate (PHB) [20]. However, only some kinds of polymers could be used to reconstruct human bone due to their flexibility and inadequate strength for severe bone loss [22].

As a thermoplastic polymer, polyetheretherketone (PEEK) is an important member of the polyaryletherketone (PAEK) family [23–25]. In the last few decades, PEEK has been used widely in clinical applications, especially in dental and cranio-maxillofacial applications (Figure 1) because of its advantages, e.g., biocompatibility, radiolucency and mechanical properties resembling human bone (Table 1) [25–28]. Compared to Ti and ceramics, the Young's modulus of PEEK are quite close to trabecular bone, which can reduce local inflammation, peri-implant bone resorption, and stress shielding problems [22,29]. The mechanical strengths of PEEK can be modified to fit the human

cortical bone by incorporation of other materials, like carbon fibers, to achieve carbon fiber reinforced PEEK composite (CFR-PEEK) [3]. In addition, PEEK has a stable aromatic structure, and pure PEEK has a melting point of around 335 °C. Thus, it could be sterilized and heated repeatedly to fit the contour of bones, which is ideal for surgical and dental instruments [30,31].

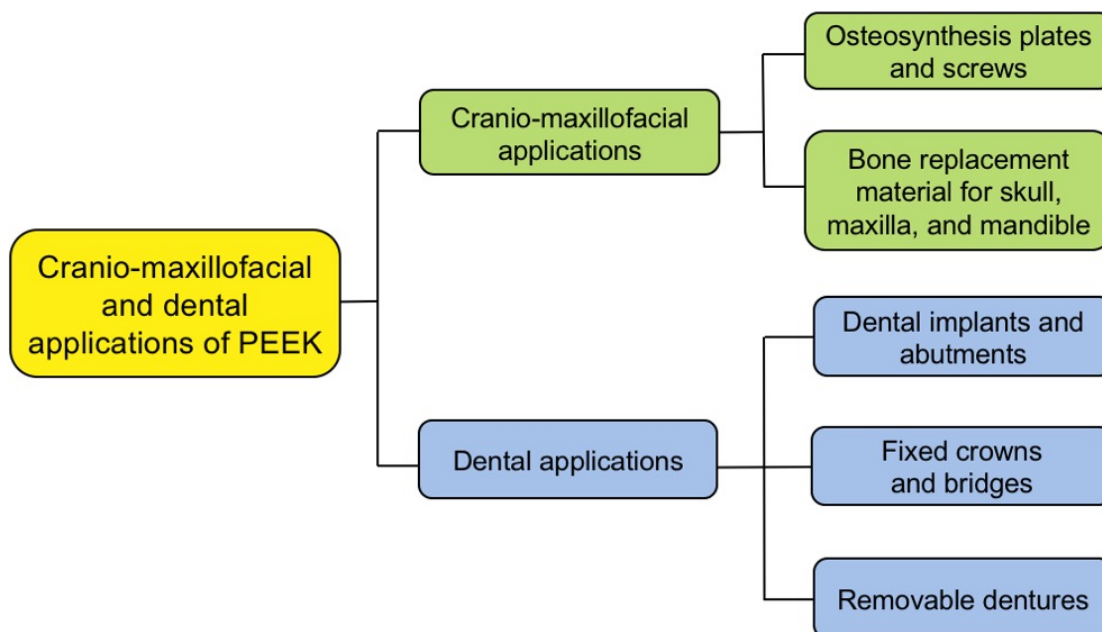


Figure 1 The dental and cranio-maxillofacial application of PEEK [3,23,27,32,33].

Table 1 The elastic modulus of PEEK, Ti, ceramics, and human tissues.

Material	Elastic modulus (GPa)	References
Cortical bone	18.6	[34]
Trabecular bone	1	[35]
PEEK	3-4	[36]
CFR-PEEK	6-8	[3]
Ti	102–110	[37]
Zirconia	210	[35]

In contrast to Ti, PEEK has very insufficient inherent osteoconductive properties, which may impede osseointegration after implantation and hamper its clinical

application [38]. Unmodified PEEK is bioinert and hydrophobic with a water contact angle of 80–90° [39]. Therefore, it is a significant challenge to overcome the bioinertness of PEEK and only make use of its potential advantages. Normally, there are two strategies to tailor the bioactivity of PEEK, e.g., surface treatment (modification) and incorporating PEEK composite. For surface treatment, there are also two methods: direct surface treatment as well as surface coating (Figure 2) [20].

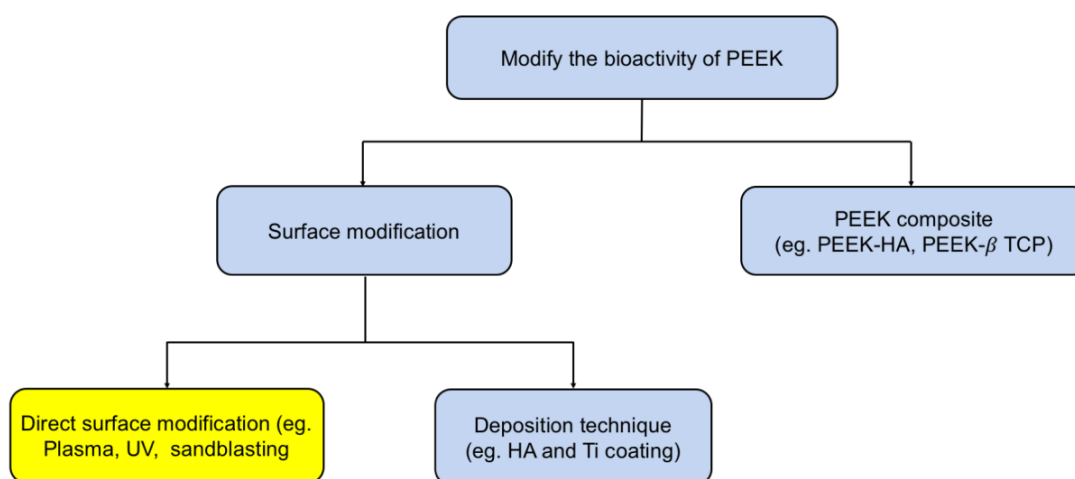


Figure 2 General strategies to improve PEEK's bioactivity.

### 1.3 Surface modification of PEEK

#### 1.3.1 Direct surface modification

Mechanical surface modification is a common way to get an ideal surface topography [40]. This treatment, including grit-blasting and polishing, is considered as a pretreatment [40]. Surface roughness is an important property for both bone implantation and restoration. Normally, surfaces with high roughness are beneficial for cell to attach and spread compared to smooth surfaces [41,42]. Besides, a rougher surface provides a larger area for cells to



attach after implantation. In the publication of Han et al. “Carbon Fiber Reinforced PEEK Composites Based on 3D-Printing Technology for Orthopedic and Dental Applications”, I compared the cytotoxicity, cell adhesion and spreading of PEEK and its composite based on fused filament fabrication (FFF) technology [3]. The result indicated that compared with polished and grit-blasted groups, the directly printed group with high roughness and special printing structures were more suitable for cells to attach [3,25]. Besides, no cytotoxic substances were introduced or produced during the printing process of the FFF technology [3].

Plasma surface modification is another way to modify the sample surfaces to improve its bioactivity. After treatment of oxygen, nitrogen, air, argon or ammonia plasma, the surface wettability of PEEK was increased a lot [43]. Waser-Althaus et al. modified the PEEK surface with O<sub>2</sub>/Ar or NH<sub>4</sub> plasma and found improved cell reactions of mesenchymal stem cell (MSC) on the sample surfaces, including cell adhesion as well as proliferation [44]. Besides, the mineralization degree was related to the power of plasma [44]. Novotna et al. modified the PEEK surface by argon plasma treatment and indicated an increase in surface wettability and changes in its surface chemistry. Besides, due to the changed surface chemistry after modification, cell reactions on the modified sample surfaces were increased significantly [45].

For dental applications, UV-A irradiation is an efficient method to increase surface wettability in case of photocatalytic titanium dioxide (TiO<sub>2</sub>) films [46]. In numerous studies, the hydrophilization effect of UV-A on TiO<sub>2</sub> have been investigated [46–48]. Funato and Jimbo indicated that, after UV-A irradiation, the protein adsorption and osseointegration accelerated compared with the control group [49,50]. Besides UV-A, UV-C irradiation is also a proper method to

improve wettability on Ti surface and showed the potential to enhance bone-implant contact during the early stage of bone healing [51,52]. However, the studies about the UV treatment of PEEK material are limited at present. Laurens et al. studied UV-C light modified PEEK surface and found that after UV-C treatment, the surface wettability and adhesive bonding properties of PEEK films increased significantly [53]. Riveiro et al. used different laser irradiation wavelength ( $\lambda = 1064, 532, \text{ and } 355 \text{ nm}$ ) to modify the PEEK samples surface, the results showed that the waviness of 355 nm had the best performance in increasing the surface hydrophilicity of PEEK [54]. Al Qahtani et al. used UV-A and UV-C to modify the PEEK implant surface, the results represented that after UV-C treatment, the surface became hydrophilized (contact angle dropped from  $109^\circ$  to  $79^\circ$ ), while after UV-A treatment, the contact angle was changed slightly only from  $109^\circ$  to  $98^\circ$  [55].

### 1.3.2 Deposition Techniques

Coating a bioactive material on the PEEK surface is a good way to tailor its bioactivity, including Ti,  $\text{TiO}_2$ , hydroxyapatite (HA), and diamond-like carbon (DLC). The most commonly-used bioactive material for PEEK coating is HA, which is a component of human bone and has ideal biocompatibility and osteoconduction [33,56]. Barkarmo compared nanocrystalline hydroxyapatite (nanoHA) coated and uncoated cylinder-shaped PEEK implants, and found that the implants coated with HA had higher surrounding bone contact rates (16% vs. 13%) compared with the uncoated group [57]. Nowadays, the most important disadvantages of coatings on PEEK are insufficient cohesion and delamination, which would influence the clinical application because the detached debris may induce local inflammation and lead to the failure of PEEK implants or restorations [58].

### 1.4 PEEK composite

Incorporation bioactive materials into PEEK objects could promote its bioactivity, e.g., TiO<sub>2</sub>, HA, strontium-containing hydroxyapatite, and  $\beta$ -tricalcium phosphate ( $\beta$ -TCP). Khor et al. fabricated a 40 vol % HA/PEEK composite and found the tensile modulus and microhardness increased in accord with the increasing HA content [59]. Converse et al. reinforced PEEK with 10 and 20 vol% HA and found evidence of brittle failure [60]. Therefore, compared with the pure PEEK, one drawback of the PEEK composite is the increased mechanical strength, which might cause stress shielding in the surrounding bone [61].

### 1.5 Additive manufacturing technology

At present, PEEK can be produced by injection molding, subtractive or additive manufacturing [AM, also called rapid prototyping (RP)] processes [62]. Compared with AM, injection molding and subtractive manufacturing have some disadvantages, e.g., time-consuming and waste of materials [63]. Besides, it is hard to finish complicated structures for subtractive manufacturing, like hollow specimens, which needs additional work by hand, and the interior of objects is always solid with subtractive manufacturing technique [64].

#### 1.5.1 A brief review of additive manufacturing

The mechanism of AM is building an object from the bottom and printing the objects layer by layer controlled by the computer [65]. Thus, different from subtractive manufacturing processes, additive manufacturing technique is a “bottom-up” format. This technique building objects in layers, which is possible to produce complex structures which cannot be achieved by subtractive manufacturing techniques [62].

Compared with subtractive manufacturing technique, AM is superior due to the advantages, like no apparent waste, no need for tooling, and enhanced cost efficiency and productivity. Besides, AM technique can create any geometry of samples, such as 3D patient specific and hollow implants. Customization and personalization may be the most significant advantages of AM for medical applications as the freedom to produce [66]. Nowadays, AM technology has been applied to various fields, such as aerospace and automobile industries, business, fashion, mechanical engineering and medical/dental applications [67]. The medical application of additive manufacturing has robustly grown over the last decades [68]. The application of AM in surgery has developed exponentially since 2013 [69]. Cranio-maxillofacial and orthopedic surgery were the first specialties to use this technology, and this is mostly because this technology is more suitable to fabricate hard tissue [70].

### **1.5.2 The classification of AM technology**

AM technology can be classified by techniques or materials. There are some representative techniques in AM, e.g., stereolithography (SLA), FFF, and selective laser sintering (SLS). The material classification includes metal powder, ceramic powder, thermoplastic, eutectic metal, alloy metal, foil, plastic film, etc. [63].

SLA is used widely in medicine to produce polymers for surgical objects, e.g., customized occlusal splints and implants [63,71]. The SLA system includes a bath of photosensitive resin, an ultraviolet (UV) laser, and a building platform. The laser is controlled by a computer for resin curing. The final objects are cured continuously by binding together the 2D layers to build a solid model from the bottom upward. Then the model will be removed from the bath and cured

additionally in a UV cabinet [72]. Generally, the accuracy of SLA is considered the greatest and has the best surface finish among AM technologies [73]. However, the most disadvantages of SLA are the limited number of materials that can be used and time-consuming processing.

SLS technique uses a CO<sub>2</sub> laser beam to build models by heating the powder particles and fusing them to create a solid layer. The laser beam moves along X and Y axes to print the structures according to the 3D data. After one layer has been finished, the build tray moves downwards to form another layer [74,75]. The manufacturing time for the SLS technique is close to the time required by SLA [76].

In the past decades, SLS was the most additive manufacturing technique to produce PEEK models [77,78]. Tan et al. fabricated PEEK-HA biocomposite scaffolds using SLS and indicated this technique as a promising approach in producing scaffolds in a higher consistency [79]. Yan et al. also used the SLS technique to produce CFR-PEEK, and found increased tensile strength and elasticity modulus compared with the injection molded bare PEEK [80].

However, high cost, low penetrability, and the concentrated laser beam restrict it from building large areas or laminates. Nowadays, FFF is one of the most popular, and mature additive manufacturing methods, which can be used for medical applications, like skull implants, osteosynthesis plates, dental implants and abutments [81].

Compared with SLS, FFF is more economical and has been used widely in medical fields in recent years. The mechanism of FFF is as follows: the melted filament is extruded from the printed nozzle, which could move in horizontal and

vertical directions controlled by the computer software [3,82]. The final model is built by fusing the layers together [82]. This process will be repeated over and over to achieve a final model.

FFF technology has many advantages, like easy material change, supervision-free operation and low maintenance costs [24]. However, there are two main weak points of FFF: the limitation of available materials and low resolution [83]. Several materials are available for FFF, like acrylonitrile butadiene styrene (ABS) and polylactic acid (PLA) [63]. Compared with PLA and ABS, PEEK has a much higher melting temperature, melting expansion and semicrystalline property, which is quite challenging to fabricate perfect performance PEEK models through FFF due to excessive thermal stress and cracks [84,85].

Therefore, PEEK needs specific parameter settings during the FFF printing process to adapt its characteristics. In 2013, Valentan et al. developed a special FFF printer with high-performance thermoplastic properties which could overcome the problems of melting and environmental temperatures to fabricate PEEK models [86]. Wu et al. measured the mechanical strength and thermal deformation performance of PEEK samples with different printing parameters by FFF technique [84]. Zhao et al. evaluated the mechanical strength and cytotoxicity of FFF-printed PEEK and found the FFF printing process would not produce or introduce toxic substances [24]. However, most of the studies focused on the manufacturing parameters, mechanical properties, and crystallinity of FFF-printed PEEK models, the information about surface wettability, topography and biological properties for medical applications are still lacking [24,81,87].

### **1.6 Aim of the study**

Some previous publications have studied the properties FFF-printed PEEK, but they all focus on the manufacturing parameters, mechanical properties, and crystallinity due to the difficulties in FFF manufacturing process [24,81,87]. Besides, the traditional manufactured PEEK surface is considered to be bioinert, the influence of FFF-printed PEEK structures and the specific surface roughness on the bioactivity of PEEK materials are still unknown.

Therefore, the aim of this research is to detect the effect of surface topography and roughness on the bioactivity of FFF-printed PEEK, e.g., osteoblasts cell adhesion, metabolic activity, and proliferation. The null hypothesis is that different PEEK surface modification methods will not influence the surface topography, wettability and bioactivity compared to untreated PEEK surfaces.

## 2 Materials and Methods

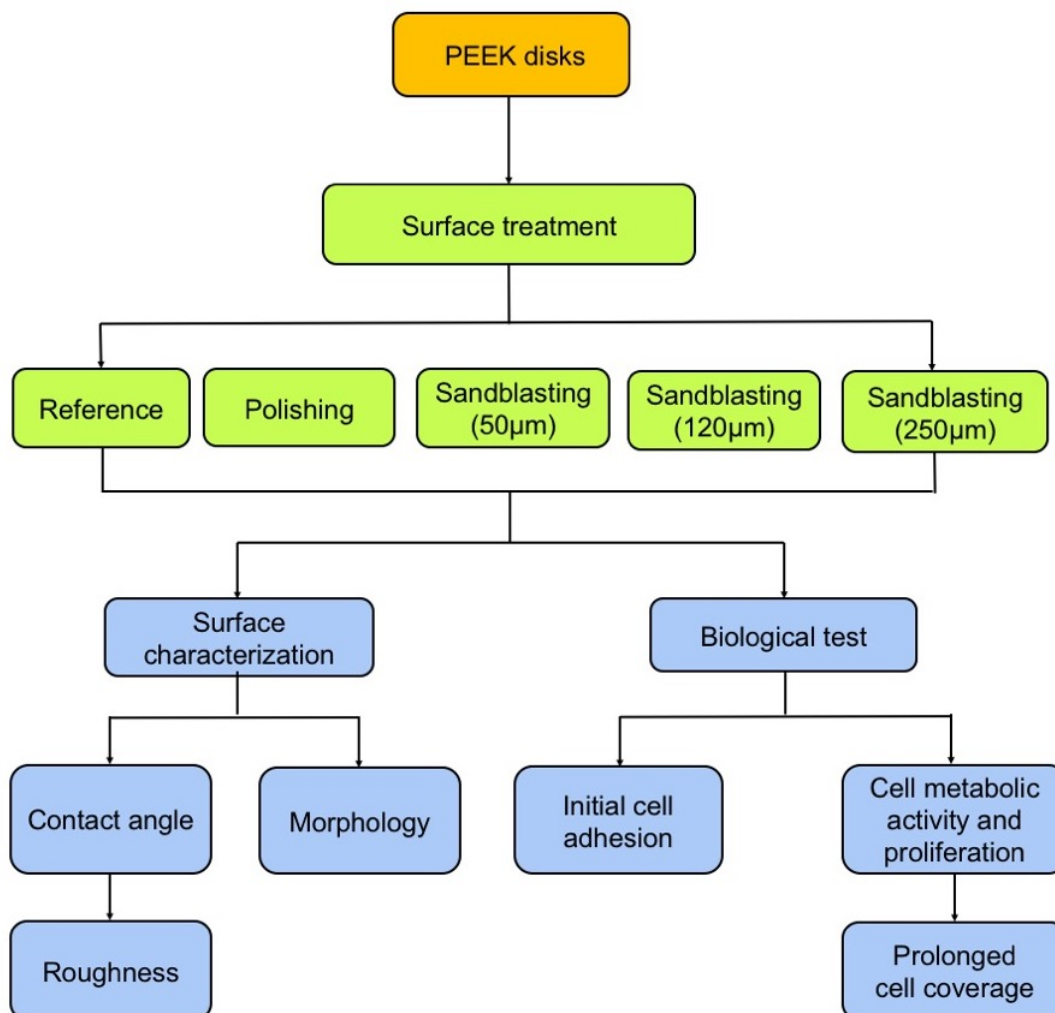


Figure 3 The flow chart of the experiment

### 2.1 PEEK samples preparation

An FFF printer was used to produce the disks (P220, Apium Additive Technologies GmbH, Karlsruhe, Germany) with the Apium Controlling Software (ACS). The technical properties and the fabricating parameters of the FFF printer are presented in Table 2 [25]. The PEEK filament used in this study is medical grade PEEK material (VESTAKEEP® i4 G resin, Evonik Resource



## 2. Materials and Methods

---

Efficiency GmbH, Essen, Germany) [25]. The properties of the filament are shown in Table 3.

PEEK disks were designed by a computer-aided design (CAD) software as an STL file. Later the file was sliced into horizontal layers by the computer slicing software, which was equal to the layers in the FFF printer. Before printing, a fixative spray (DimaFix, DIMA 3D, Valladolid, Spain) was applied to the print platform to increase the adhesion of samples. The molten PEEK material was extruded by the printing nozzle and deposited on the printing bed in layers. After one layer was finished, the working bed dropped down to let the new layer to deposit. During producing, the entire chamber was enclosed to achieve the recommended print head and bed temperature (480°C and 130 °C).

After printing, the support parts of the PEEK disks were removed manually. Then the samples were cleaned and disinfected ultrasonically with deionized (DI) water and 70 % ethanol (Sonorex super RK102H, Bandelin, Germany) to remove the fixative spray left on the sample surfaces and eliminate the influence of it on biological tests [25].

Table 2 Technical properties and the fabricating parameters of the printer [25].

Description	Value
Layer Thickness	0.1mm
Print Head	480° C
Print Bed	130° C
Nozzle Diameter	0.4 mm

Table 3 The material properties of PEEK filament [25].

Description	Value
Melting range	340 °C
Density	1.30 g cm <sup>-3</sup>
Tensile Modulus	3500 MPa
Stress at yield	96 MPa
Strain at yield	5%

---

### 2.2 Surface modification of PEEK samples

In this study, there were three kinds of PEEK samples, untreated (n = 40), polished (n = 40), and grit-blasted disks (n = 120, n = 40 for each subgroups) [25]. Samples of the polishing and grit-blasting groups were polished with increasing SiC abrasive papers (1200, 2,500, and 4000 grit Buehler, Lake, Bluff, IL, USA) [25]. For the grit-blasting groups, alumina (Al<sub>2</sub>O<sub>3</sub>) particles of different grain sizes (Cobra, Renfert, Hilzingen, Germany, 50 µm, 120 µm, and 250 µm) were used to get different surface roughness. The grit-blasting parameters were as follow:

Distance: 50 mm; time: 15 s; pressure: 0.1 MPa (P-G 400, Harnisch+Rieth, Winterbach, Germany, Figure 4) [25].

After surface modification, all the samples were cleaned ultrasonically with DI water and 70 % ethanol (15 min for each) respectively and dried by nitrogen. Then, the disks were steam sterilized in an autoclave (WESA, Brussels, Belgium, 134°C, 5 min) before testing.

## 2. Materials and Methods

---

After cleaning and sterilization, the samples were packed in sterile bags and the bags were sealed for later testing of wettability and bioactivities, including initial cell adhesion, cell metabolic activity, and cell proliferation.



Figure 4 Grit-blasting machine.

### 2.3 Surface characterization

#### 2.3.1 Scanning electron microscopy (SEM)

Surface topography of the PEEK surfaces was visually displayed by an SEM device (LEO 1430, Zeiss, Oberkochen, Germany, Figure 5). First, the samples were sputtered with a sputter coater (SCD 050, Baltec, Lübeck, Germany). The sample surfaces were coated with a current of 60 mA for 100 s to achieve a 20 nm thickness Au-Pd coating. After coating, samples were placed into the SEM device under an accelerating voltage of 20 kV in a vacuum. Representative areas for the different sample surfaces were photo-documented at 200 ×, 1000 ×, 2000 ×, and 10000 × magnification.



Figure 5 SEM device.

### 2.3.2 Analysis of surface topography

Six samples were investigated for each surface type. The surface roughness of PEEK disks was analyzed by the profilometry (Perthometer S6P, Mahr, Göttingen, Germany, Figure 6). First, the disks were fixed horizontally on the platform. A needle tip moves in X and Y axes across the disk surface at 0.5 mm/s speed. The measuring area is  $3 \times 3$  mm with 121 profiles for the roughness analysis. A surface analysis software (Mountainsmap Universal, Digital Surf, France) was used to calculate the two-dimensional roughness parameters ( $R_a$ ,  $R_q$ ,  $R_z$ ,  $R_t$ ,  $R_{sk}$ , and  $R_{ku}$ ). The original data were filtered through a robust Gaussian filter (ISO 16610-71) and the cut-off value was set at  $600 \mu\text{m}$  [88].

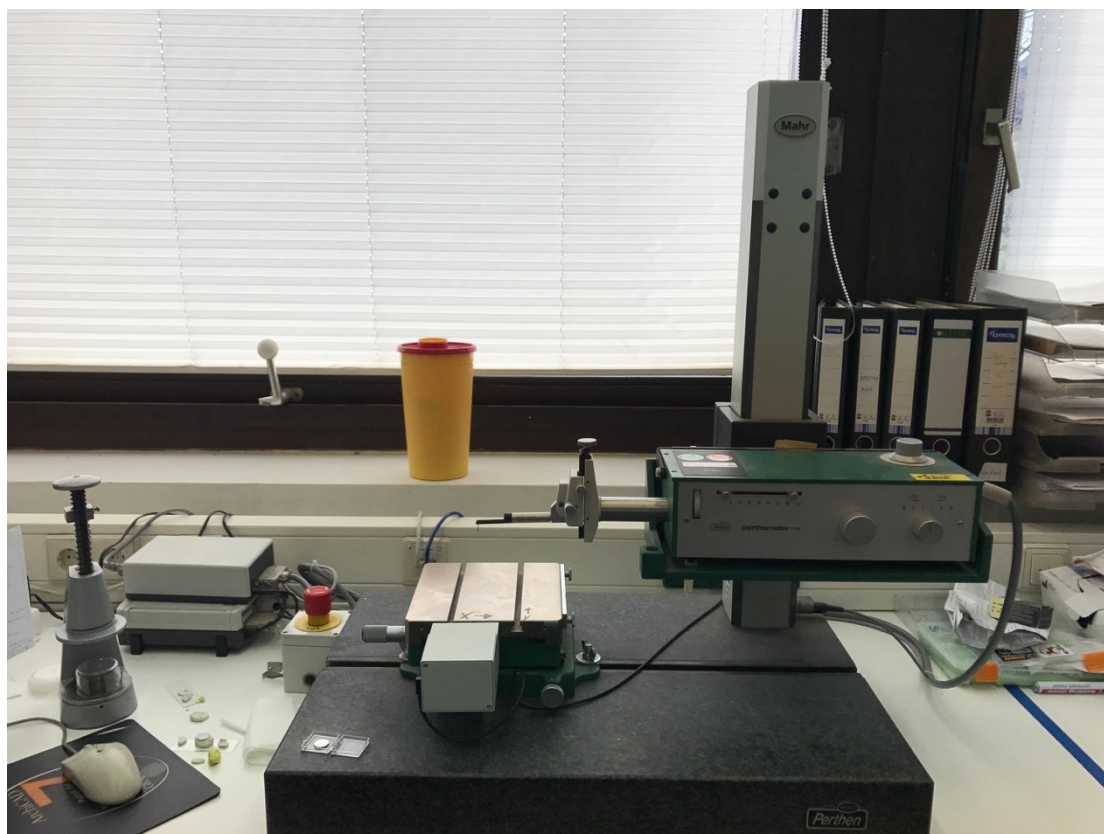


Figure 6 Surface topography measurement system (profilometer).

Table 4 Description of two-dimensional roughness parameters [89–91].

Name	Symbol	Description	Mathematical
<b>arithmetical mean deviation of the assessed profile</b>	$R_a$	arithmetic mean of the absolute ordinate values $Z(x)$ within a sampling length	$R_a = \frac{1}{l} \int_0^l  Z(x)  dx$
<b>Root mean square deviation of the roughness profile</b>	$R_q$	root mean square value of the ordinate values $Z(x)$ within a sampling length	$R_q = \sqrt{\frac{1}{l} \int_0^l Z^2(x) dx}$
<b>Maximum height of the roughness profile</b>	$R_z$	sum of height of the largest profile peak height $Z_p$ and the largest profile valley depth $Z_v$ within a sampling length	$R_z = \max(Z(x)) + \min(Z(x))$
<b>Total height of profile</b>	$R_t$	sum of the height of the largest profile peak height $Z_p$ and the largest profile valley depth $Z_v$ within the evaluation length	$R_z = \max(Z_{pi}) + \min(Z_{vi})$
<b>Skewness of the assessed profile</b>	$R_{sk}$	quotient of the mean cube value of the ordinate values $Z(x)$ and the cube of $R_q$ within a sampling length	$R_{sk} = \frac{1}{R_q^3} \left[ \frac{1}{l} \int_0^l Z^3(x) dx \right]$
<b>Kurtosis of the assessed profile</b>	$R_{ku}$	quotient of the mean quartic value of the ordinate values $Z(x)$ and the fourth power of $R_q$ within a sampling length	$R_{ku} = \frac{1}{R_q^4} \left[ \frac{1}{l} \int_0^l Z^4(x) dx \right]$

### 2.3.3 Sessile-drop contact angle measurement

The water contact angle on the sample surfaces were measured by a high-resolution drop shape analysis device ( $n = 6$  / group, DSA 10-MK 2, DSA 10-MK 2, Krüss, Hamburg, Germany, Figure 7). The of ultrapure water was used for testing with a sessile drop of 2  $\mu\text{L}$  for each measurement. The whole wetting process was video-controlled, and the videos were saved by the DSA calculation software (version 1.90.0.11, Krüss, frame rate: 25 frame/s), and the contact angle in the air-water-substrate interface (after 20 seconds wetting time) was measured from the drop geometry analysis.





Figure 7 Drop shape analysis device.

### 2.4 Biological tests

The biological tests contain cell adhesion, metabolic activity and proliferation. Before cell cultivation, the disks were cleaned and sterilized as described above. (See section 2.2).

#### 2.4.1 Osteoblast cell culture

SAOS-2 osteoblasts cell line (DSMZ GmbH, Braunschweig, Germany) was used for this experiment. Cell culture flasks were used for culturing the SAOS-2 osteoblasts (CellBind T-75, Corning, Tewksbury, MA, USA) [25]. The culture medium was prepared by McCoy's 5A medium (Sigma-Aldrich, USA), 15% fetal bovine serum (FBS, Life Technologies Co., Carlsbad, CA, USA), 1% penicillin

and streptomycin (15140-122, Life Technologies Co.), and 1% L-glutamine (GlutaMAX, Life Technologies Co.) [25]. The cells were cultured in an incubator, and the culturing conditions are: temperature: 37 °C; atmosphere: 5% CO<sub>2</sub>; humidity: 95%. The medium was replaced twice a week [25].

For harvesting, the adherent cells on the flask bottom were separated by 1.5 ml trypsin- EDTA (0.05% trypsin/0.02% EDTA, Life Technologies Co.) for 5 min in the incubator [25]. Then 10 ml of cell culture medium were used to stop the reaction, and 10 µl of the new medium was taken to count the cells number. The total number of cells was counted by a hemocytometer chip (DHC-N01, NanoEnTek, San Diego, CA, USA), a mechanical piece counter (T123 IVO, Checkline Europe, Enschede, Netherlands) and a microscope (CK2, Olympus, Tokyo, Japan).

### 2.4.2 Initial cell adhesion

The inoculating cell density was about  $1.5 \times 10^5$  cells/cm<sup>2</sup> using a 24-well plate (Cluster, Corning, Tewksbury, MA, USA). For each well, the growth area was 2 cm<sup>2</sup>. Therefore, the total cell number for each well was  $3 \times 10^5$  and the volume of culture medium was 1.2 ml. According to the result of pre-test experiments, the cultivation time was set to 4 h for the initial cell adhesion test.

After cleaning and sterilization, the PEEK disks were put into 24-well plates. There were 4 samples and 4 background controls for each group (untreated; polished; 50 µm, 120 µm, and 250 µm Al<sub>2</sub>O<sub>3</sub> grit-blasted), so 40 disk samples for each independent test [25]. Four vacant wells with cells only were applied as tissue culture polystyrene (TCPS) controls. The cell number required for each experiment was  $7.2 \times 10^6$  cells for 20 samples and 4 TCPS controls. The disks were placed and fixed in the middle of the well with sterile wax, and the cell



## 2. Materials and Methods

---

suspensions were seeded on the surfaces of samples. Then the plate was put into the incubator and incubated for 4 hours.

After incubation for 4 hours, the medium from the wells was carefully removed by jet pump suction. Each well of the 24-well plate was rinsed with 500  $\mu$ l Hank's Salt Solution (Biochrom AG, Berlin, Germany) [25]. Then the adhered cells were fixed with 500  $\mu$ l 3% paraformaldehyde (MERCK, Haar, Germany) in dulbecco's phosphate-buffered saline (DPBS, Gibco, Paisley, UK) for 15 minutes [25]. After fixation, the paraformaldehyde solution was removed and discarded [25]. Then, each well was stained with 500  $\mu$ l crystal violet dye (Sigma-Aldrich, Steinheim, Germany), the staining time was also 15 min [25]. After staining, the crystal violet dye was removed, and the PEEK disks were rinsed five times with distilled water (500  $\mu$ l / well), respectively, and transferred into new plates. Optical micrographs of the sample surfaces were taken by a microscope (M400, Wild Heerbrugg, Gais, Switzerland) using a digital camera (EOS 500D, Canon, Tokyo, Japan).

After taking pictures, the cell-staining dye on the sample surfaces was solubilized with 500  $\mu$ l pure methanol (MERCK, Haar, Germany) for 15 minutes at room temperature [25]. After discoloration, 100  $\mu$ l of the dissolved solution from each well of the 24-well plate was transferred into a 96-well plate, and four transferred wells for each sample were used. The absorbance was measured at 550 nm in an ELISA reader (Tecan F50, Tecan Austria, Groedig, Austria). The mean values of the background control group were subtracted from the corresponding sample values.

The total test was repeated two times. The OD values, referring to the untreated group, were calculated. Therefore, the modified mean OD value of the as printed

group was set to 100%, and the OD values of other groups were divided by this value.

### **2.4.3 Cell metabolic activity and proliferation assay**

Four samples from each group (untreated, polished, 50  $\mu\text{m}$ , 120  $\mu\text{m}$ , and 250  $\mu\text{m}$   $\text{Al}_2\text{O}_3$  grit-blasted) were placed and fixed in the middle of the well with sterile wax, and the cell suspensions were seeded on the sample surfaces. Four vacant wells only with cells were applied as TCPS proliferation controls, and four other wells were used as blank controls and contained neither samples nor cells (only medium).

The seeding density of SAOS-2 cells was  $3 \times 10^4$  cells/ $\text{cm}^2$  on the experimental samples and TCPS controls. Therefore, the cell number for a well was  $6 \times 10^4$ , and the medium volume is 1.2 ml. The total cell number required for each experiment was  $1.44 \times 10^6$  cells for 20 samples and 4 TCPS controls. Since the diameter of the 24-well plates was 16 mm, and the diameter of the samples was 14 mm, the samples almost covered the bottom completely. This proper size of well and samples could ensure that the majority of cells were seeded on the sample surfaces.

After incubation for 1 d, 3 d, and 5 d, for each well, 600  $\mu\text{l}$  of the medium was removed, and 60  $\mu\text{l}$  CCK-8 labeling reagent (Dojindo Molecular Technologies, Inc., Rockville, MD, USA) was added [25]. After an additional incubation for 3 hours, 100  $\mu\text{l}$  mixture of the CCK-8 reagent and the medium from each well of the 24-well plate was transferred into a 96-well plate. Four wells in the 96-well plate were used for each sample. The optical density (OD) was then measured spectrophotometrically using the ELISA reader at 492 nm wavelength (reference

wavelength: 620 nm). The culture medium was changed every time after each measurement. The total test was repeated four times.

### **2.4.4 Surface coverage measurement**

At the end of the last CCK-8 measurement (five days), the experimental samples, TCPS controls, blank controls, and background controls in the proliferation assay were subjected to the cell coverage measurement. The measurement steps were the same as described in section 2.4.2.

The whole test was repeated four times. The OD values, referring to the untreated group, were calculated. Therefore, the modified OD value of the as printed group was set to 100%, and the OD values of other groups were divided by this value.

### **2.5 Statistical analysis**

SPSS software (version 25, SPSS INC, Chicago, IL, USA) was used in this study for data analysis. The data distribution and homogeneity of variances were analyzed by Shapiro–Wilk and Levene tests. One-way analysis of variance (ANOVA) followed by Tukey post-hoc test was applied for comparing differences among groups (untreated, polished, 50  $\mu\text{m}$ , 120  $\mu\text{m}$ , and 250  $\mu\text{m}$   $\text{Al}_2\text{O}_3$  grit-blasted groups) ( $\alpha = 0.05$ ).  $P < 0.05$  was considered a significant statistical difference.

### 3 Results

#### 3.1 Surface characterization

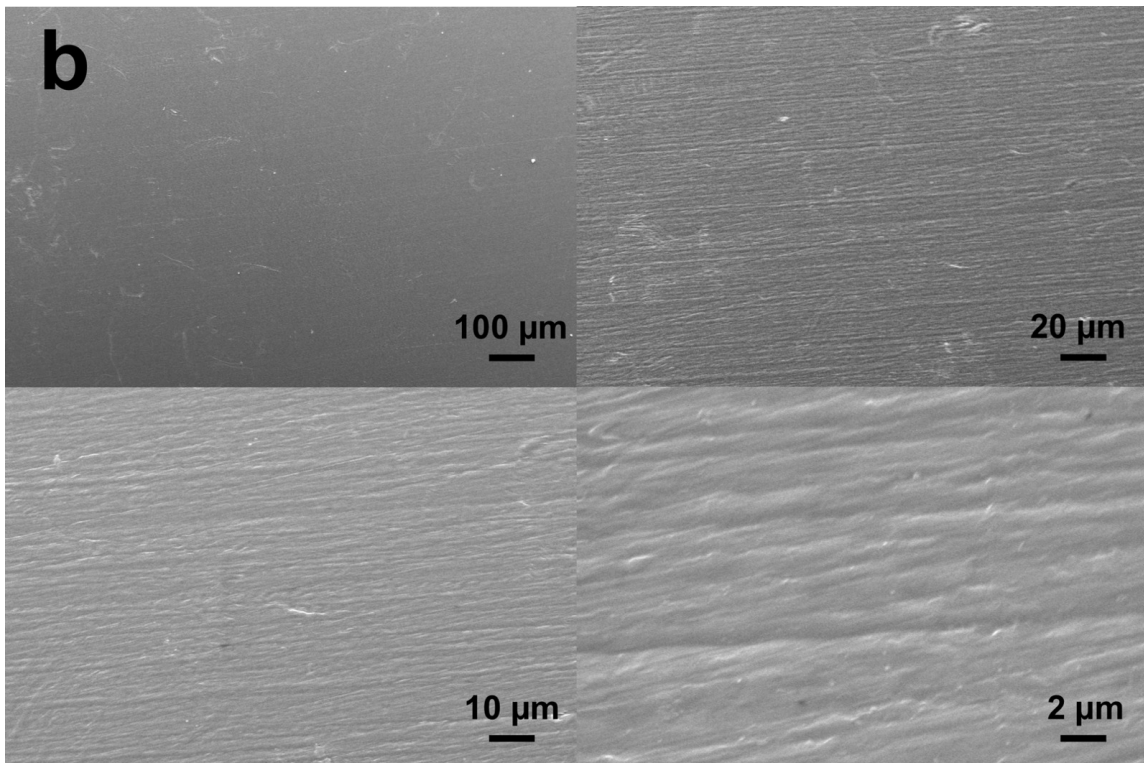
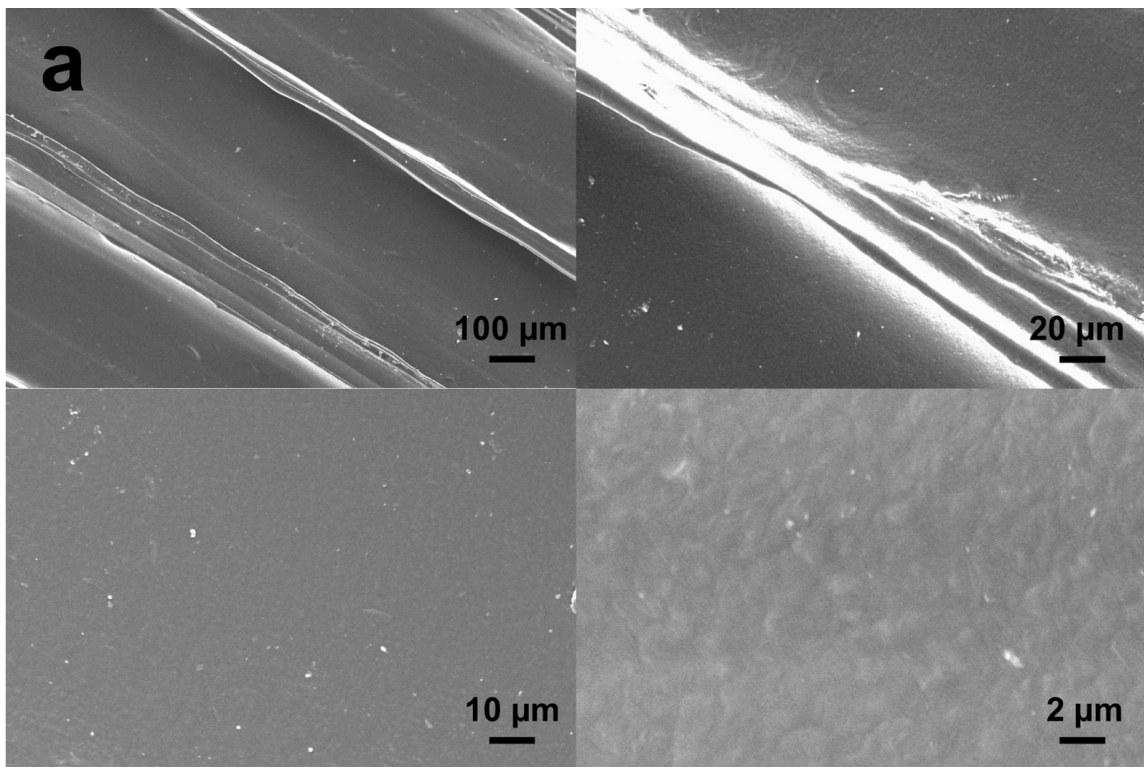
##### 3.1.1 Surface morphology characterization

To understand how surface topological factors affect the bioactivities of FFF-printed PEEK materials, first, the surface morphology of sample surfaces were determined using SEM. Figure 8 indicates the SEM images of PEEK sample surfaces of different groups (untreated, polished, 50  $\mu\text{m}$ , 120  $\mu\text{m}$ , and 250  $\mu\text{m}$   $\text{Al}_2\text{O}_3$  grit-blasted groups).

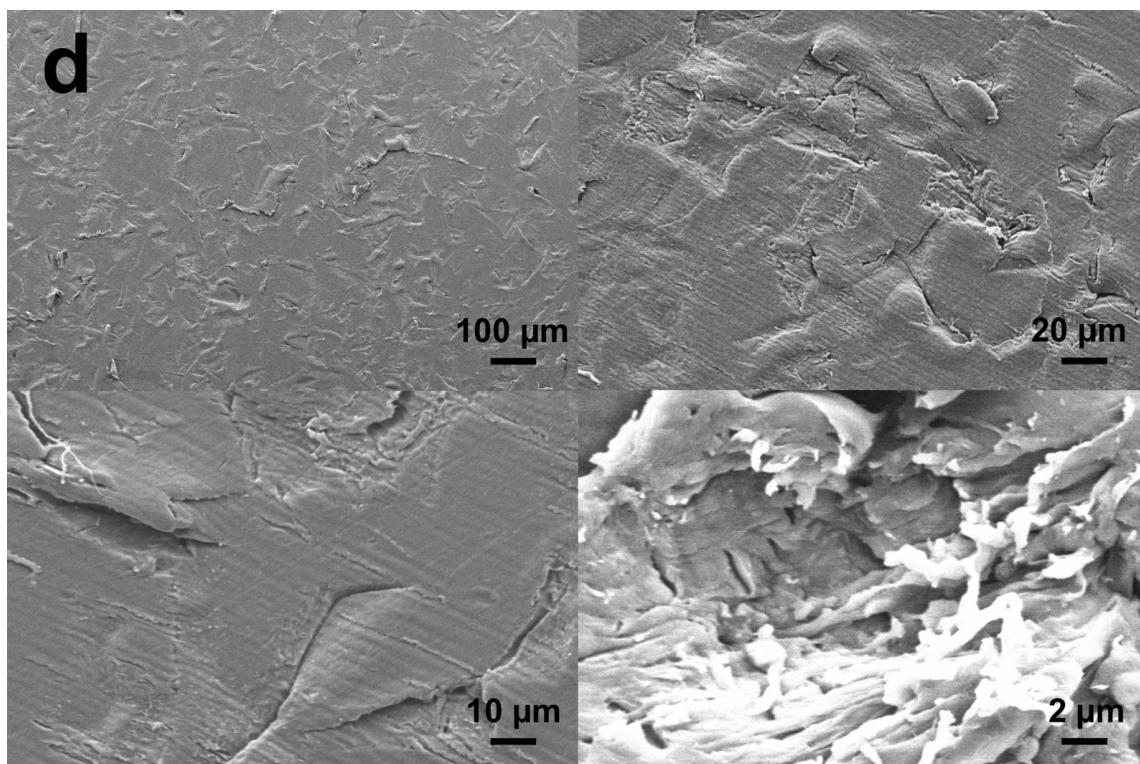
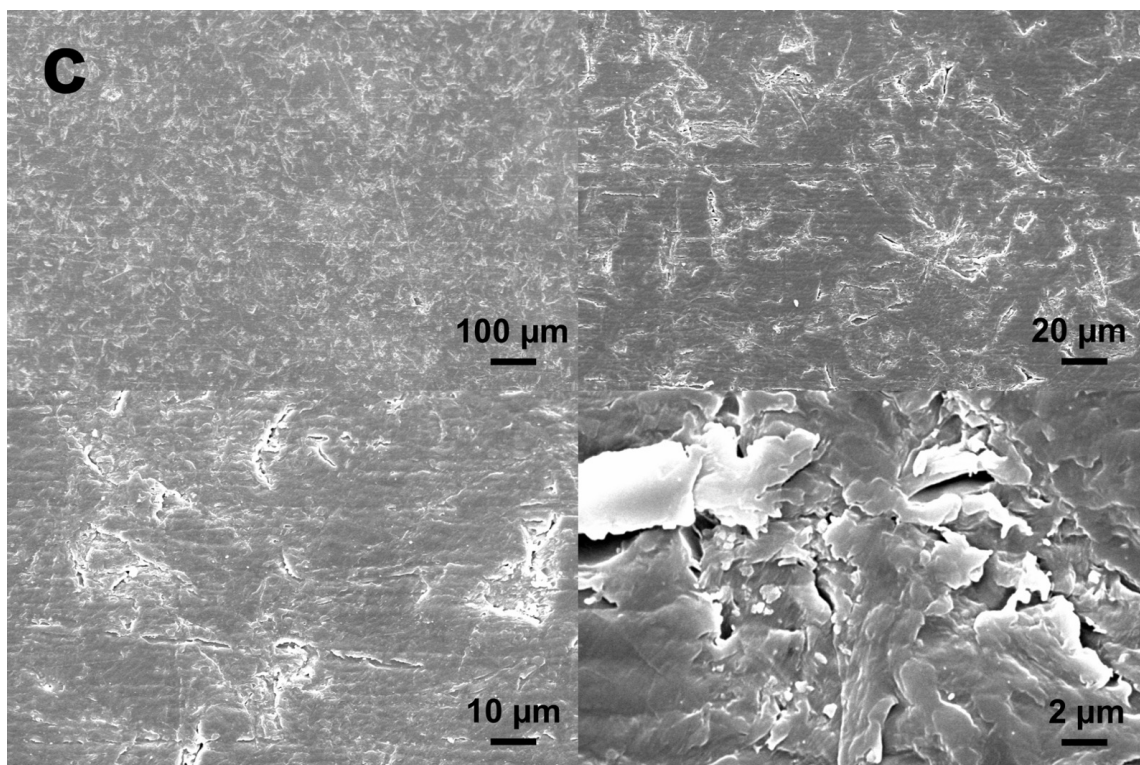
For the untreated samples, the printing structures were obvious due to the FFF manufacturing pattern (Figure 8a). Distinct peaks and valleys of the waveforms on the sample surfaces could be observed [25]. After polishing, the specific printing lines disappeared completely and left homogenous and smooth surfaces (Figure 8b) [25]. The grit-blasted surfaces didn't show the printing structures either. Compared with polished surfaces, the grit-blasted surfaces possessed micrometer surface features covering the surfaces with homogeneously with protuberances and cavities, leading to a micrometer rough surface topography (Figure 8c-10e) [25]. Besides, the surface micro-roughness raised with the increase in the grit-blasted  $\text{Al}_2\text{O}_3$  particle size. Larger and more protuberances and cavities were observed on the 250  $\mu\text{m}$   $\text{Al}_2\text{O}_3$  modified sample surfaces compared with the 50  $\mu\text{m}$  and 120  $\mu\text{m}$   $\text{Al}_2\text{O}_3$  grit-blasted samples.

### 3. Results

---



### 3. Results



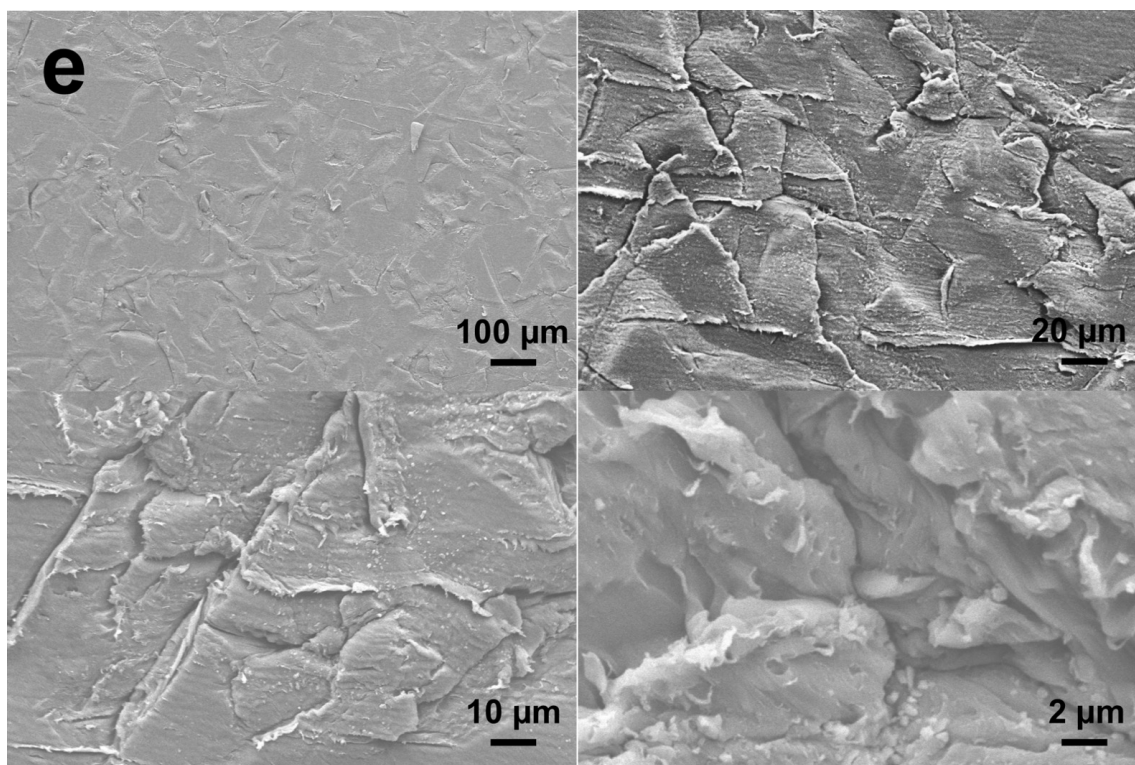


Figure 8 SEM images of different sample groups under 200 $\times$ , 1000 $\times$ , 2000 $\times$ , and 10000 $\times$  magnification. (a) directly printed PEEK; (b) polished PEEK; (c) 50  $\mu\text{m}$   $\text{Al}_2\text{O}_3$  particle grit-blasted PEEK; (d) 120  $\mu\text{m}$   $\text{Al}_2\text{O}_3$  particle grit-blasted PEEK; (e) 250  $\mu\text{m}$   $\text{Al}_2\text{O}_3$  particle grit-blasted PEEK.

### 3.1.2 Surface roughness characterization

The surface topography and roughness of the different groups were investigated by profilometry. The roughness result ( $R_a$ ,  $R_q$ ,  $R_z$ ,  $R_t$ ,  $R_{sk}$ , and  $R_{ku}$ ) and the reconstructed 3D surface topographies are shown in Table 5 and Figure 9. The amplitude parameters of the untreated group as chosen in this study ( $R_a$ ,  $R_q$ ,  $R_z$ , and  $R_t$ ) indicated that the untreated PEEK samples showed significantly higher roughness values than the polished and grit-blasted samples ( $p < 0.05$ ) [25]. Besides, the differences between the polished and three grit-blasted groups were not significant ( $p > 0.05$ ). Figure 9 showed the statistical charts of the roughness parameters. In addition, the roughness values of the grit-blasted PEEK related to the grain diameter of the  $\text{Al}_2\text{O}_3$  particles, which in accord with the observation from SEM [25].

### 3. Results

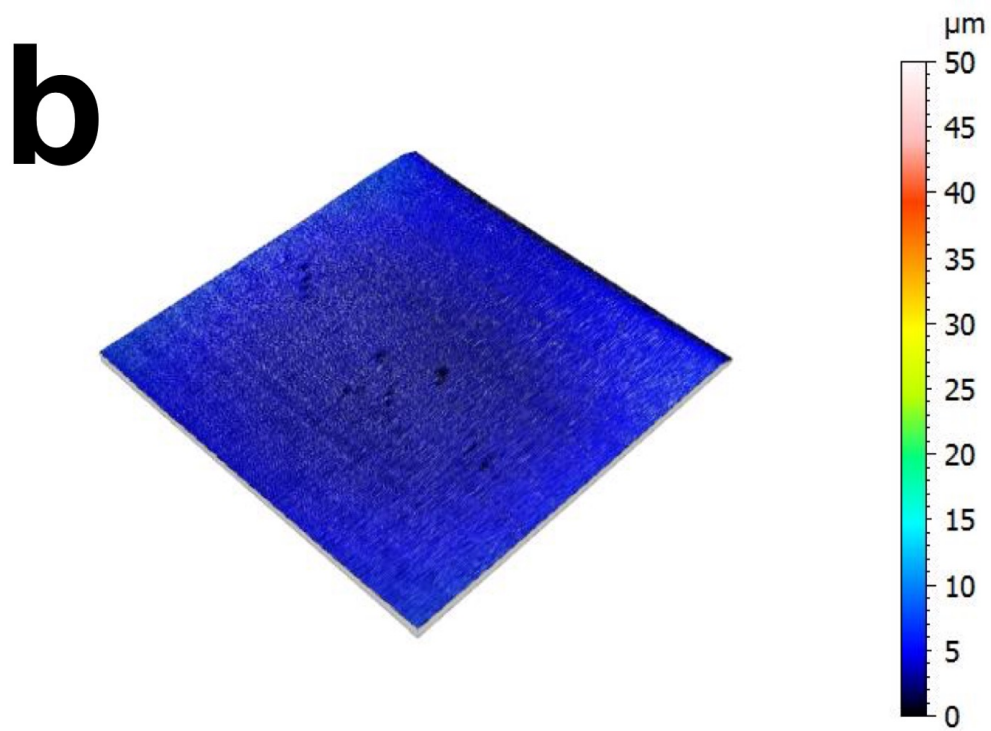
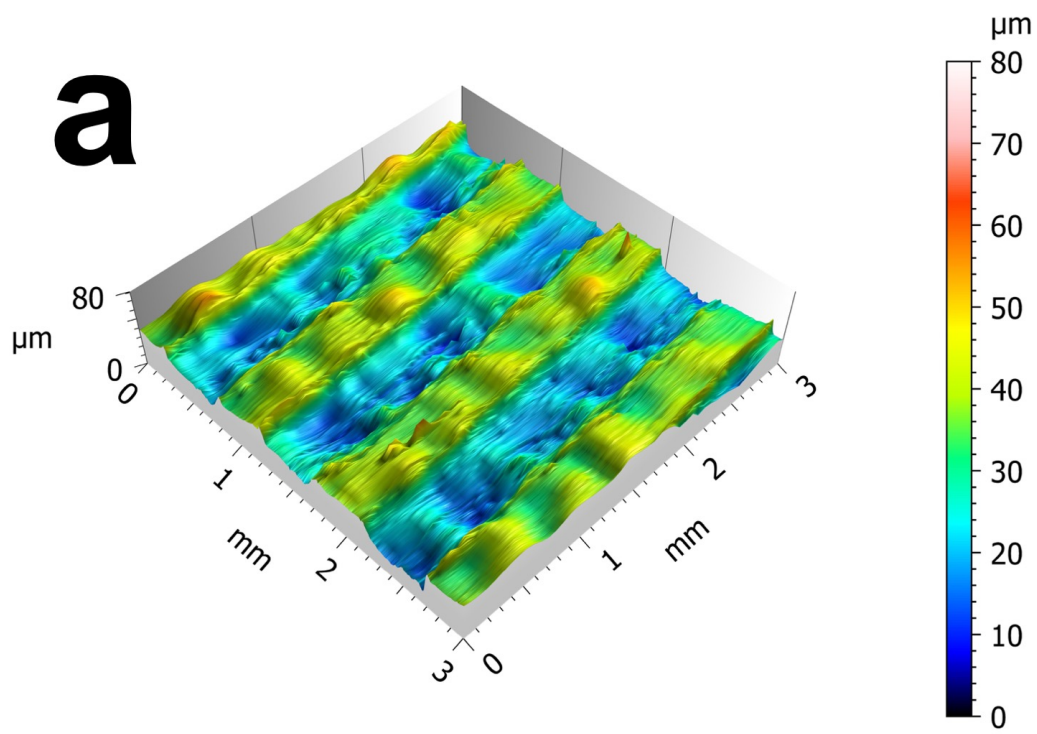
Table 5 Roughness characterization (means  $\pm$  standard deviations).

Group	R <sub>a</sub> ( $\mu\text{m}$ )	R <sub>q</sub> ( $\mu\text{m}$ )	R <sub>z</sub> ( $\mu\text{m}$ )	R <sub>t</sub> ( $\mu\text{m}$ )	R <sub>sk</sub> (/)	R <sub>ku</sub> (/)
Untreated	22.28 $\pm$ 15.26 <sup>a</sup>	26.75 $\pm$ 17.17 <sup>a</sup>	83.23 $\pm$ 48.52 <sup>a</sup>	110.71 $\pm$ 56.45 <sup>a</sup>	0.83 $\pm$ 0.19 <sup>a</sup>	3.13 $\pm$ 0.84 <sup>a</sup>
Polished	0.17 $\pm$ 0.08 <sup>b</sup>	0.30 $\pm$ 0.15 <sup>b</sup>	1.60 $\pm$ 0.69 <sup>b</sup>	4.33 $\pm$ 2.35 <sup>b</sup>	-0.19 $\pm$ 0.18 <sup>b</sup>	6.41 $\pm$ 1.09 <sup>b</sup>
Grit-blasted (50 $\mu\text{m}$ )	0.28 $\pm$ 0.13 <sup>b</sup>	0.49 $\pm$ 0.25 <sup>b</sup>	3.13 $\pm$ 1.20 <sup>b</sup>	6.28 $\pm$ 3.29 <sup>b</sup>	-0.24 $\pm$ 0.22 <sup>b</sup>	8.20 $\pm$ 0.82 <sup>b</sup>
Grit-blasted (120 $\mu\text{m}$ )	0.43 $\pm$ 0.15 <sup>b</sup>	0.76 $\pm$ 0.23 <sup>b</sup>	5.07 $\pm$ 1.18 <sup>b</sup>	9.88 $\pm$ 2.58 <sup>b</sup>	-0.62 $\pm$ 0.15 <sup>b</sup>	10.89 $\pm$ 1.82 <sup>c</sup>
Grit-blasted (250 $\mu\text{m}$ )	0.52 $\pm$ 0.38 <sup>b</sup>	0.88 $\pm$ 0.56 <sup>b</sup>	5.72 $\pm$ 3.12 <sup>b</sup>	10.34 $\pm$ 5.18 <sup>b</sup>	-0.37 $\pm$ 0.68 <sup>b</sup>	10.90 $\pm$ 2.70 <sup>c</sup>

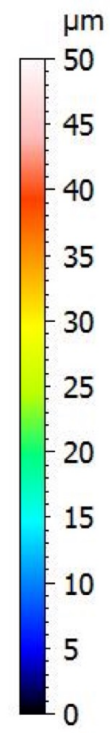
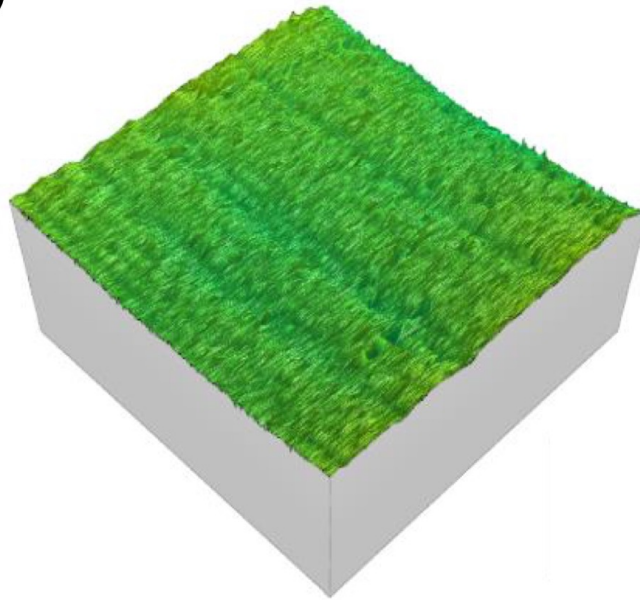
Different lowercase letters in the same column indicate significantly different groups ( $p < 0.05$ ).

Skewness (Rsk) and kurtosis (Rku) are also amplitude parameters, representing the asymmetry and sharpness of peaks and valleys. Normally, Rsk=0 means the peaks and valleys are symmetrical to the average line (normal distribution). In this study, the Rsk value for the untreated PEEK was significantly higher compared to others with a value greater than zero. This indicated the predominance of valleys comprising these surfaces. As for other groups, the values were quite similar and all less than zero, which meant that peaks account for the majority on these surfaces. The Rku value in the grit-blasted groups with 120  $\mu\text{m}$  and 250  $\mu\text{m}$  Al<sub>2</sub>O<sub>3</sub> particles showed a higher value compared with others ( $p < 0.05$ ). Also, the Rku value in the untreated group was the ( $p < 0.05$ ). Theoretically, Rku=3 meant normal distribution, and Rku>3 indicated the height distribution is sharp. In this study, all the groups were higher than three, which indicated the sharp height distribution, but 120  $\mu\text{m}$  and 250  $\mu\text{m}$  grit-blasted groups were sharper than the polished and 50  $\mu\text{m}$  grit-blasted groups, and the untreated group had the bluntest peaks or extreme deep valleys on sample surfaces [25].

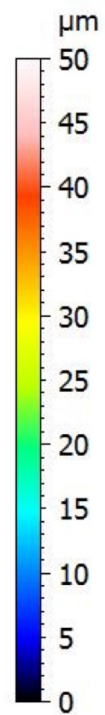
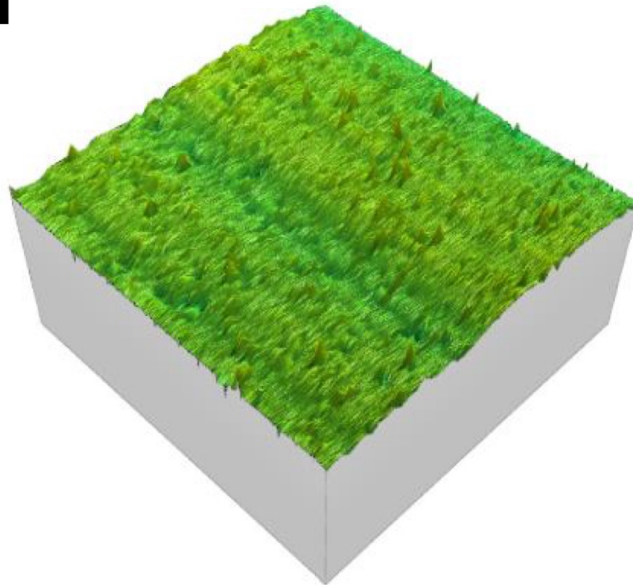




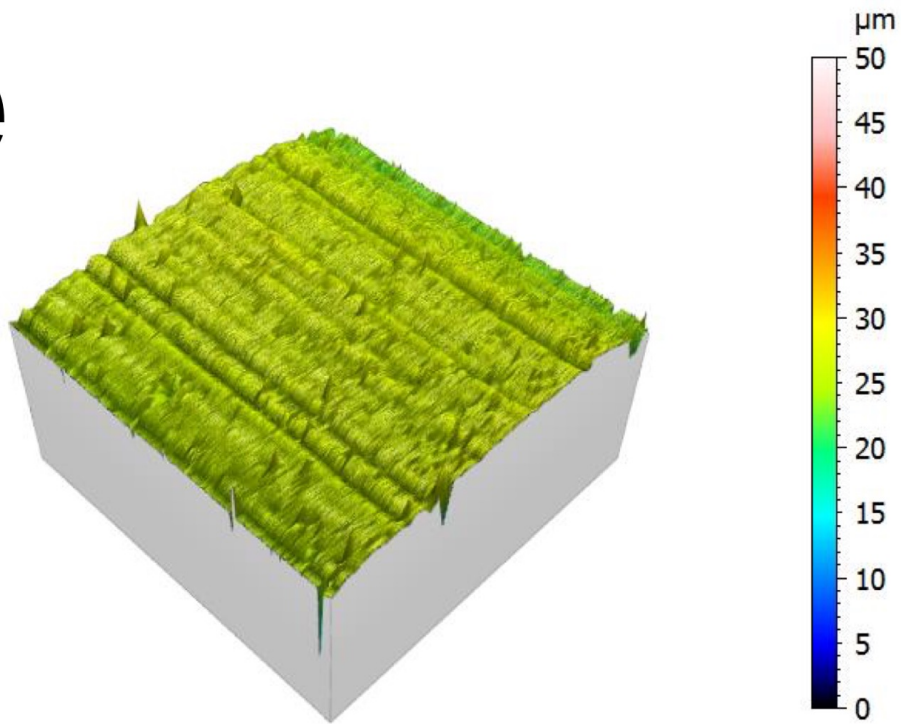
**c**



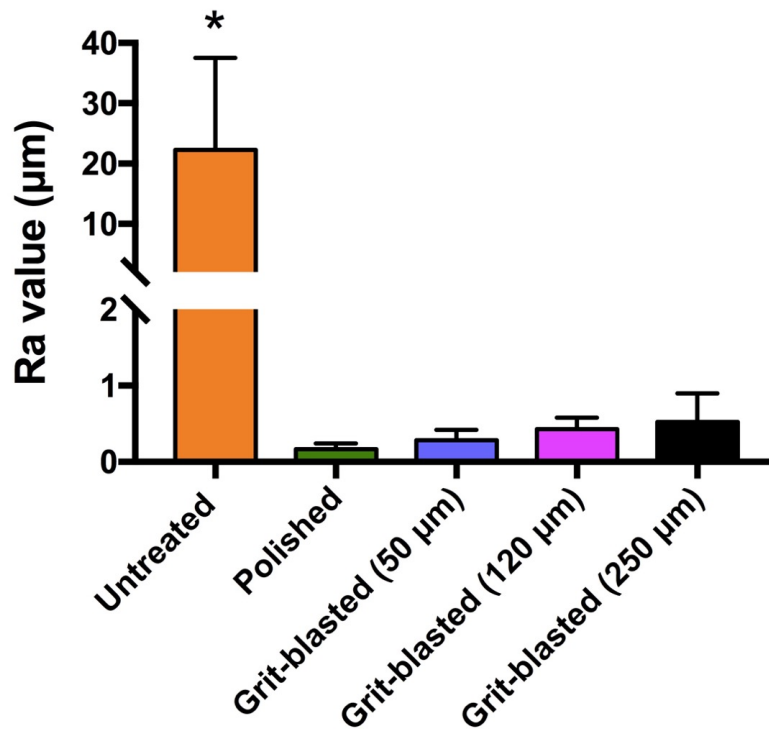
**d**

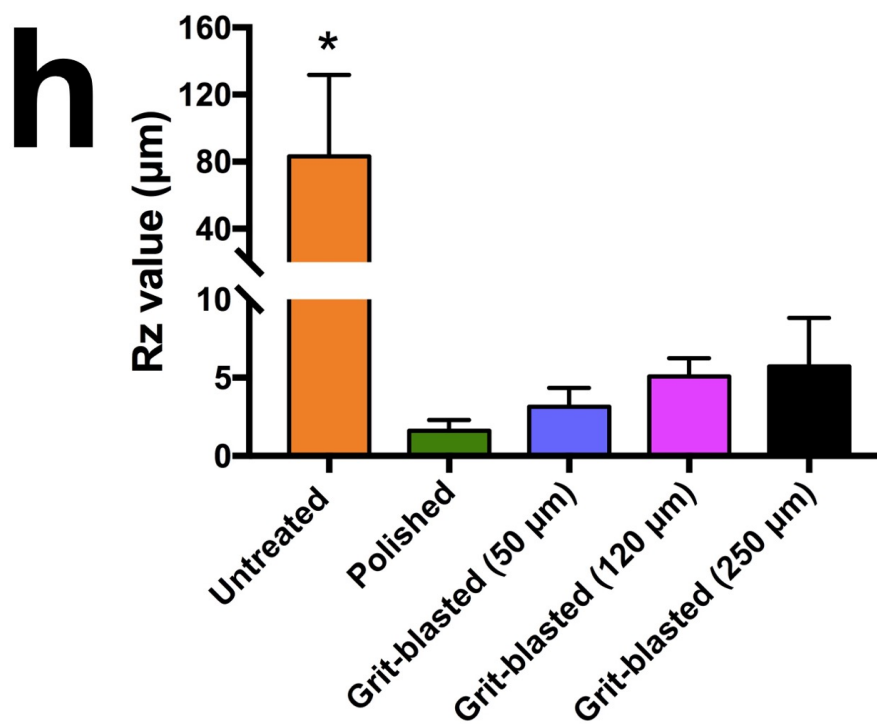
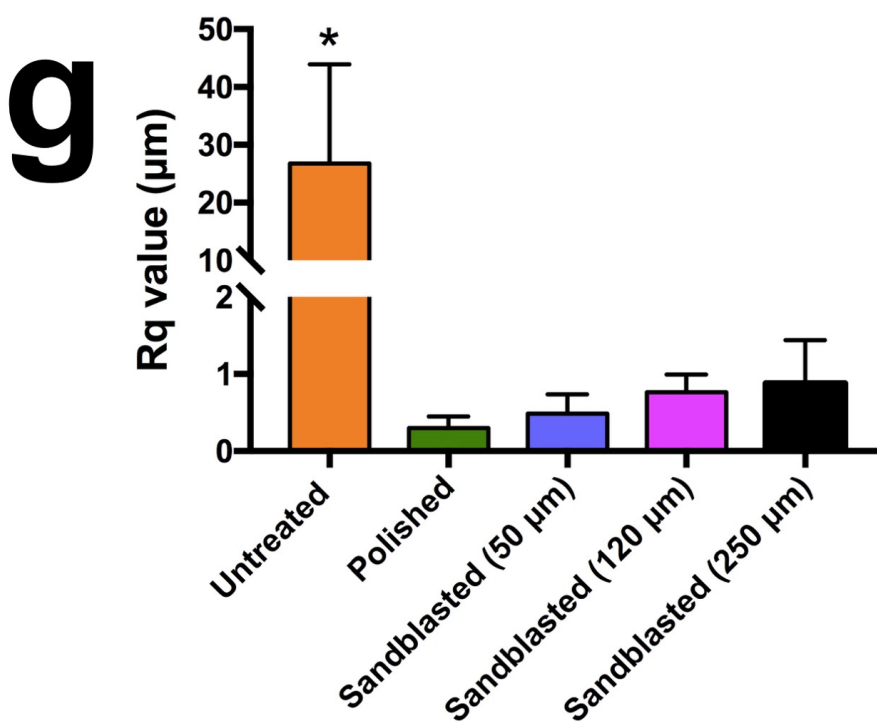


**e**

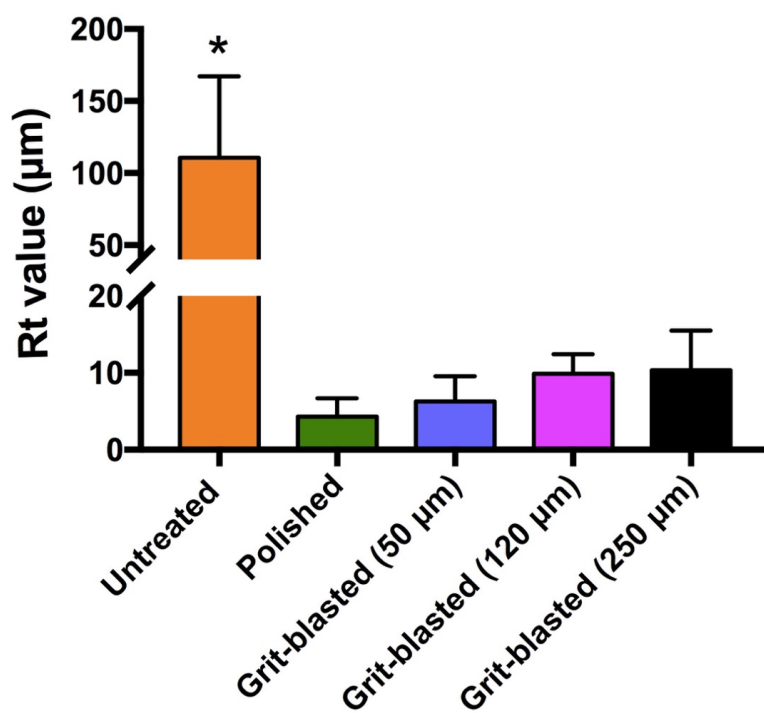


**f**

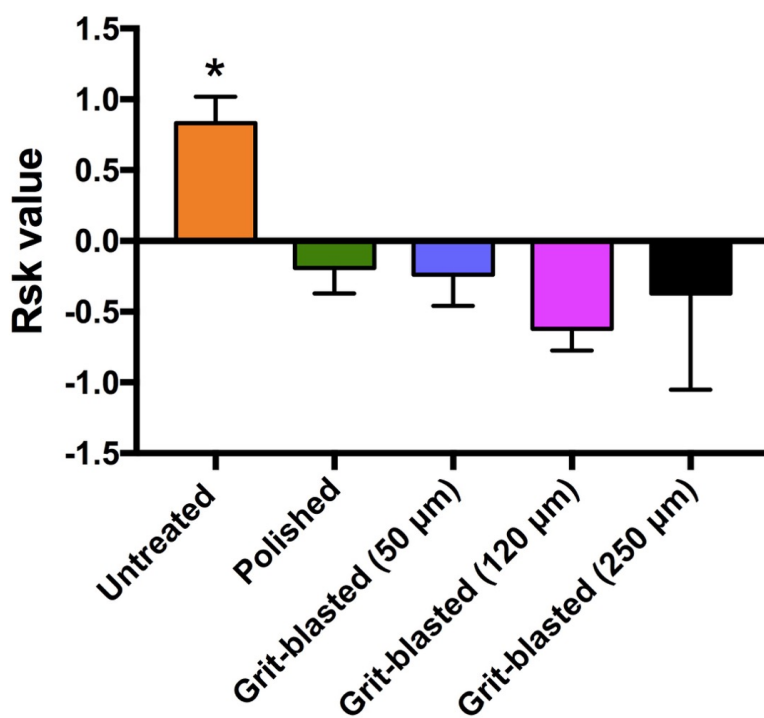




**i**



**j**



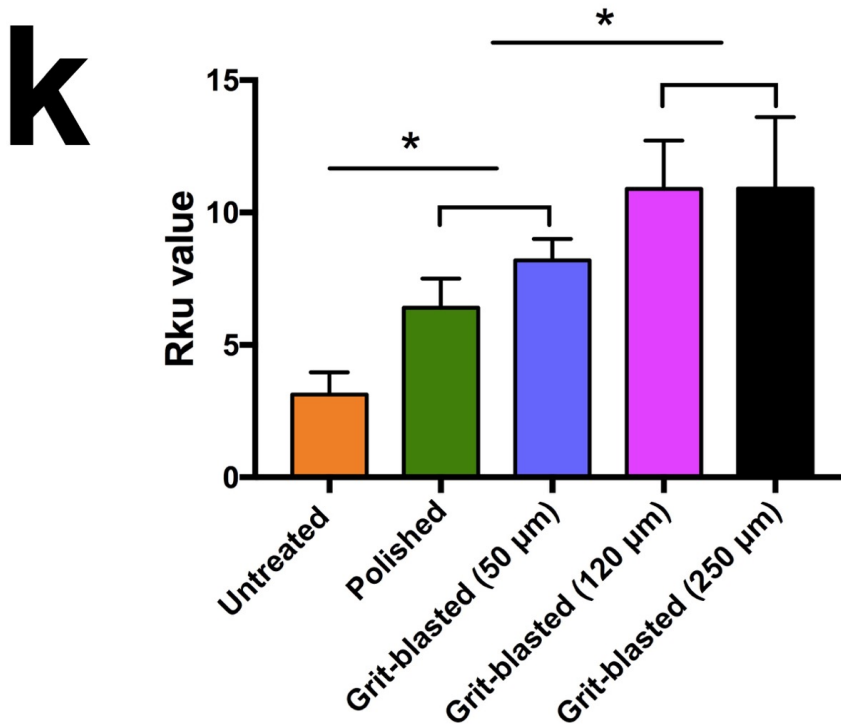
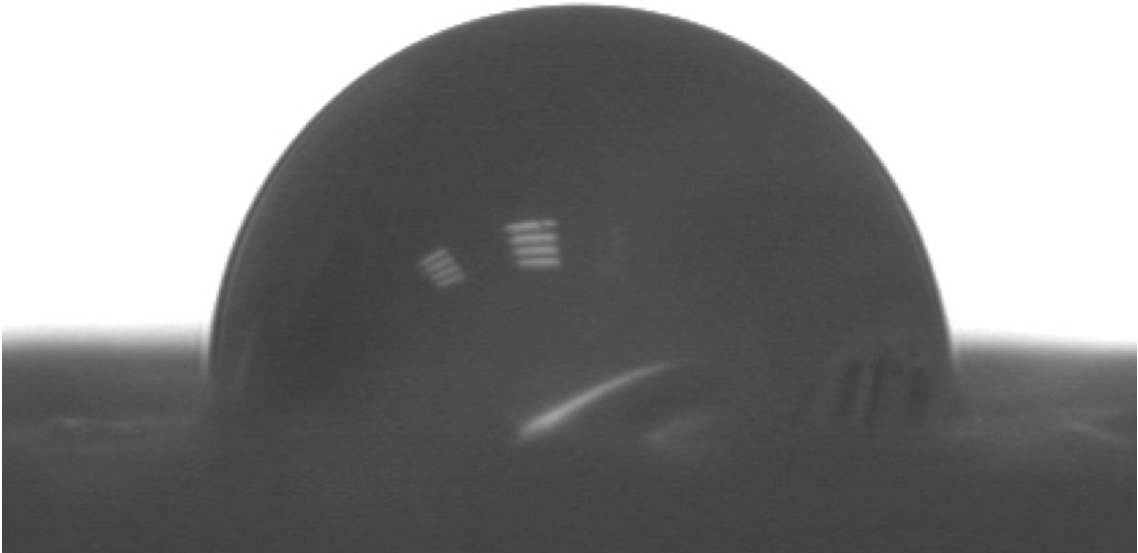


Figure 9 Reconstructed 3D surface roughness topography and different 2D parameter values. values: (a) directly printed PEEK; (b) polished PEEK; (c) 50  $\mu\text{m}$   $\text{Al}_2\text{O}_3$  particle grit-blasted PEEK; (d) 120  $\mu\text{m}$   $\text{Al}_2\text{O}_3$  particle grit-blasted PEEK; (e) 250  $\mu\text{m}$   $\text{Al}_2\text{O}_3$  particle grit-blasted PEEK; (f) Ra values; (g) Rq values; (h) Rz values; (i) Rt values; (j) Rsk values; (k) Rku values. \*  $p < 0.05$ .

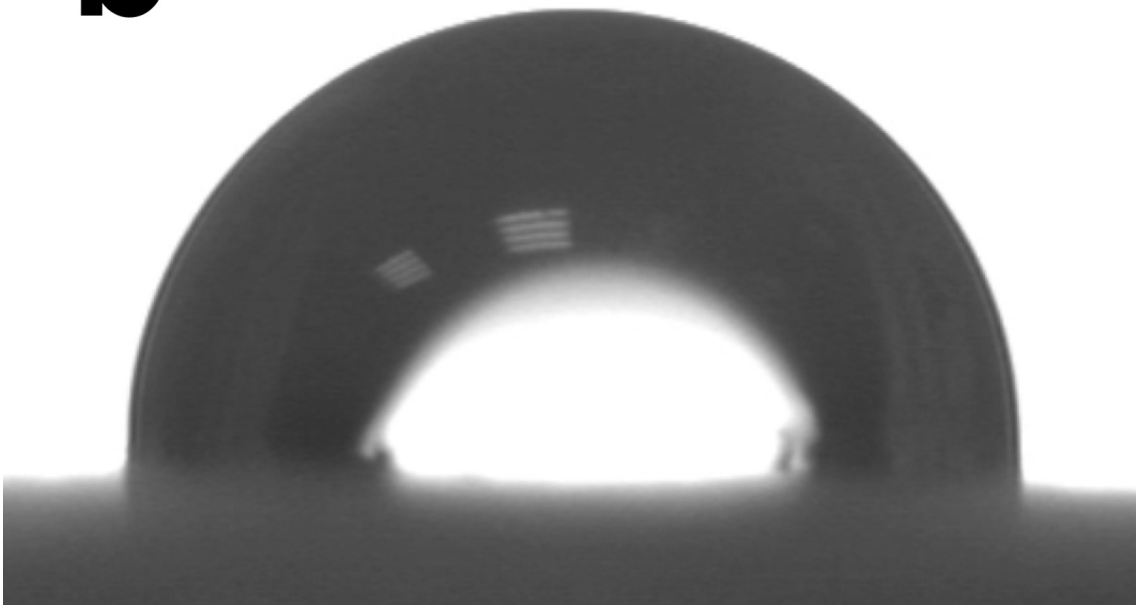
### 3.1.3 Contact angle measurement

The result of contact angle measurements is presented in Figure 10. Data indicated that all the groups, no matter with or without surface treatment, revealed a slightly hydrophilic behavior with a contact angle less than  $90^\circ$  (Untreated samples:  $84.6 \pm 9.6^\circ$ , Polished samples:  $86.5 \pm 4.4^\circ$ , 50  $\mu\text{m}$   $\text{Al}_2\text{O}_3$  grit-blasted samples:  $88.7 \pm 3.0^\circ$ , 120  $\mu\text{m}$   $\text{Al}_2\text{O}_3$  grit-blasted samples:  $88.0 \pm 2.2^\circ$ , 250  $\mu\text{m}$   $\text{Al}_2\text{O}_3$  grit-blasted samples:  $87.1 \pm 3.5^\circ$ ) [25]. But there were no significant differences among different sample surfaces ( $p < 0.05$ ), which meant that after surface modification, the wettability didn't change obviously.

**a**

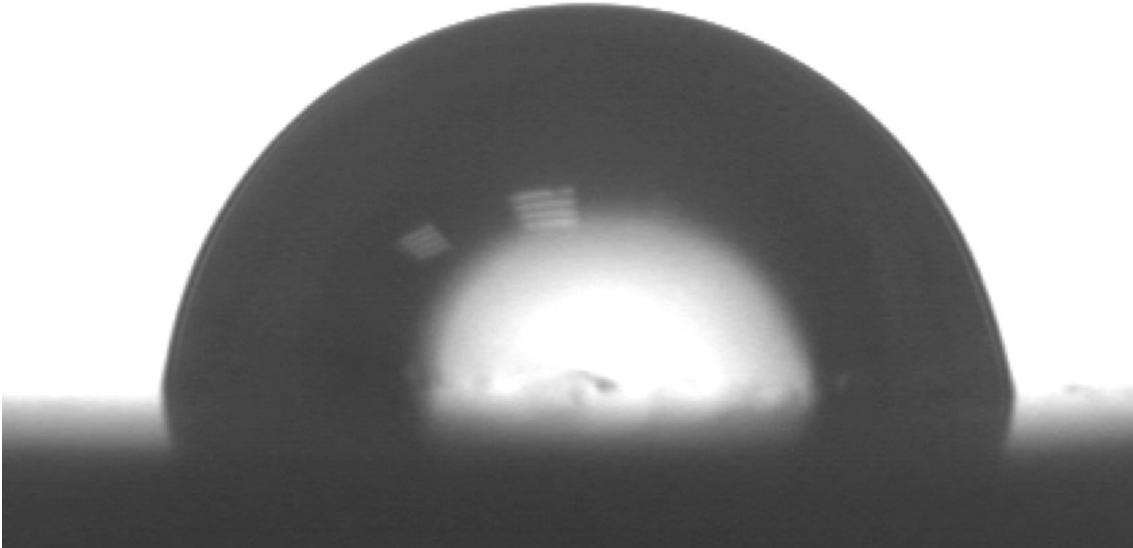


**b**

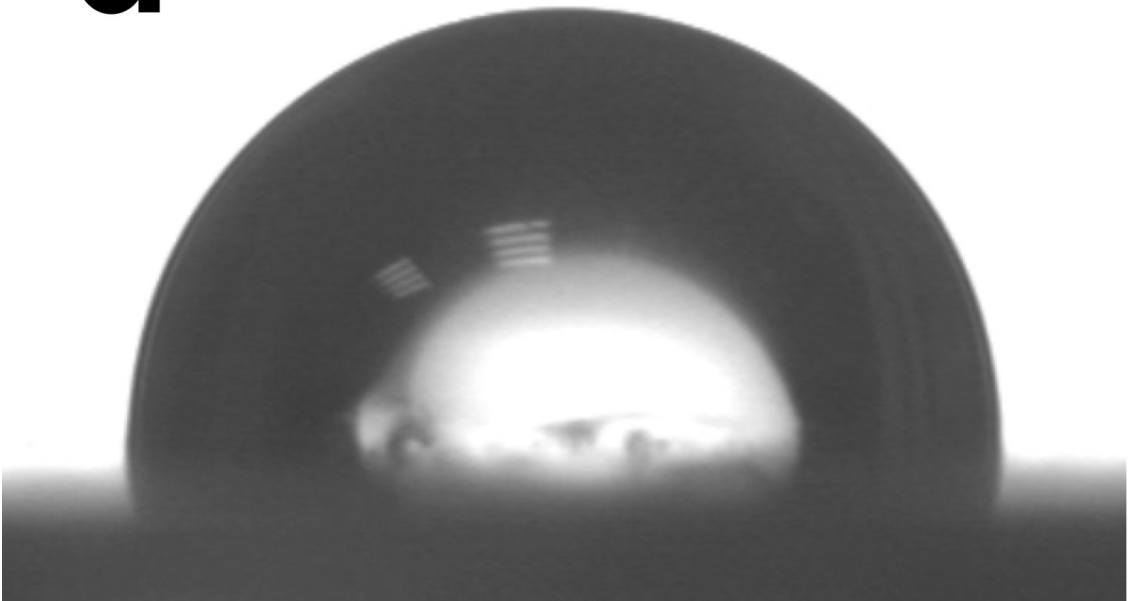




**C**



**d**





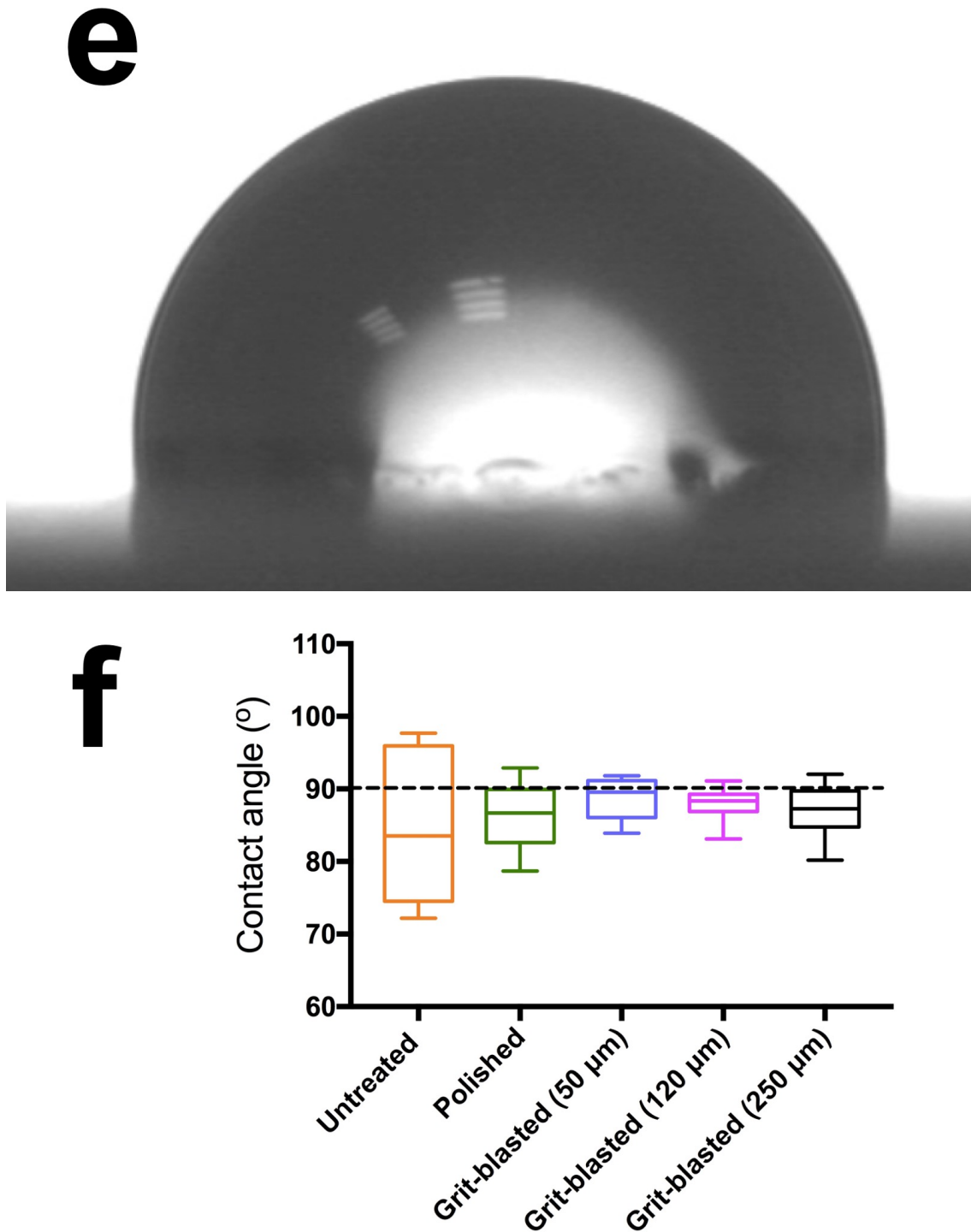
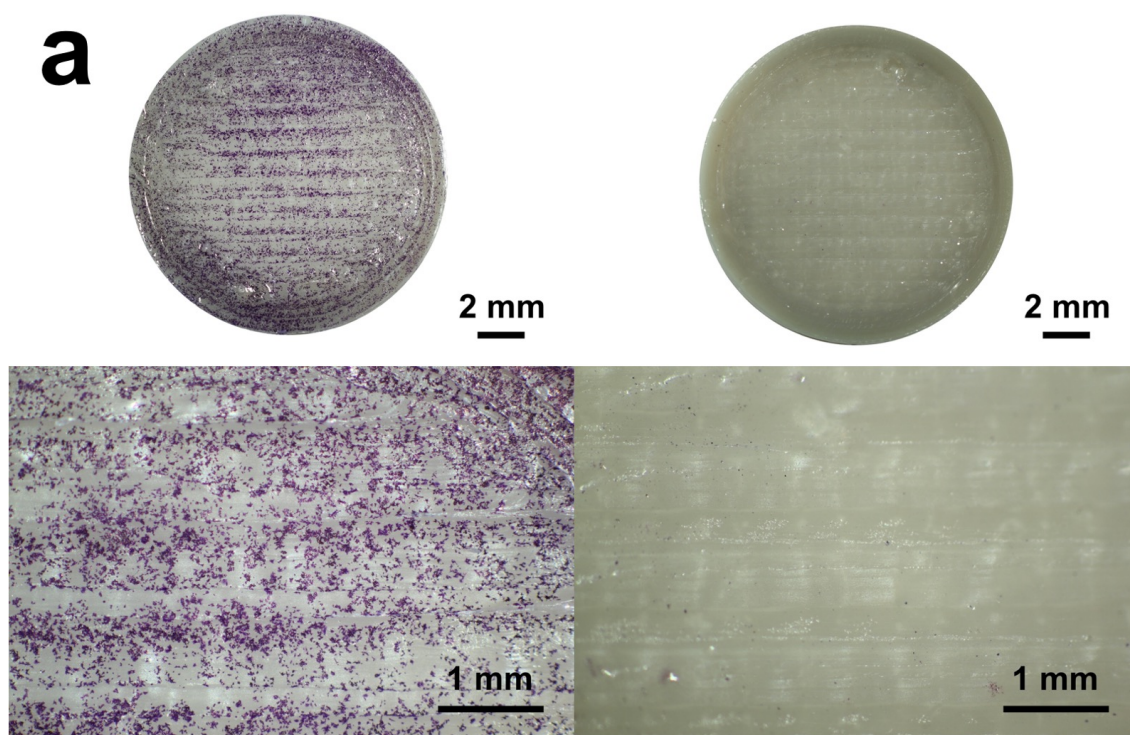


Figure 10 Water contact angles measurement: (a) directly printed PEEK; (b) polished PEEK; (c) 50  $\mu\text{m}$   $\text{Al}_2\text{O}_3$  particle grit-blasted PEEK; (d) 120  $\mu\text{m}$   $\text{Al}_2\text{O}_3$  particle grit-blasted PEEK; (e) 250  $\mu\text{m}$   $\text{Al}_2\text{O}_3$  particle grit-blasted PEEK; (f) the quantitative result of the contact angle. The dotted line ( $90^\circ$ ) shows the borderline between hydrophilicity and hydrophobicity [25].

### 3.2 Biological tests

#### 3.2.1 Initial cell adhesion

Figure 11 and Figure 12 shows the result of initial cell adhesion test. The result represented a similar cell adhesion on different sample surfaces. The microscopic images revealed that there was not a big difference in the surface coverage by SAOS-2 cells after four hours' incubation (Figure 11). The quantitative result confirmed this finding. Although for the 250  $\mu\text{m}$  grit-blasted group, it showed a slightly higher osteoblastic surface coverage than in for the other groups (Figure 12, modified OD value: untreated group:  $100 \pm 10\%$ , polished group:  $101 \pm 14\%$ , 50  $\mu\text{m}$  grit-blasted group:  $107 \pm 13\%$ , 120  $\mu\text{m}$  grit-blasted group:  $118 \pm 21\%$ , and 250  $\mu\text{m}$  grit-blasted group:  $137 \pm 45\%$ ), but the standard deviation in this group was also higher than in the other groups [25].



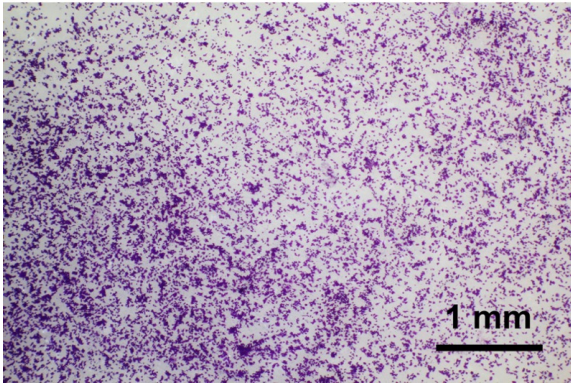
**b**



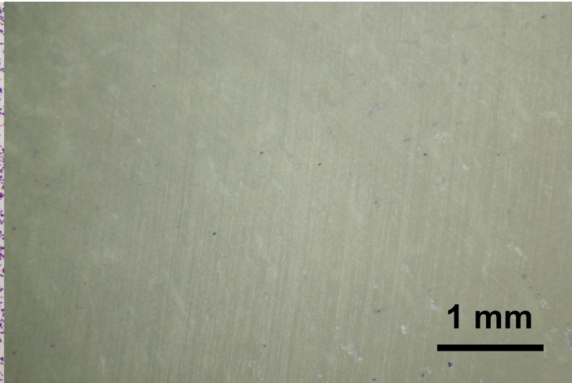
2 mm



2 mm

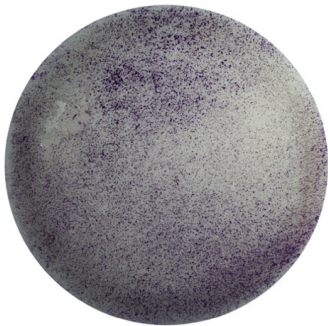


1 mm



1 mm

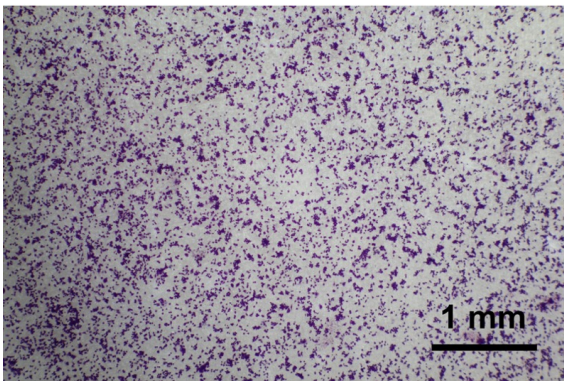
**c**



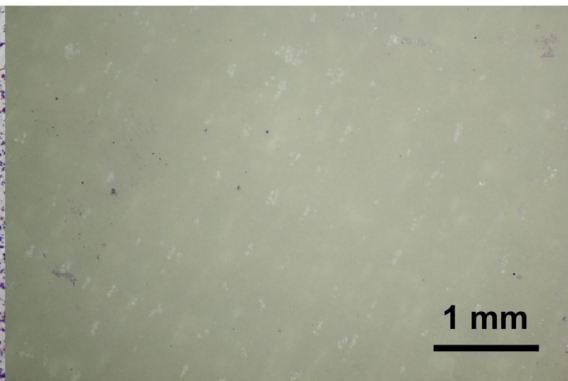
2 mm



2 mm



1 mm



1 mm



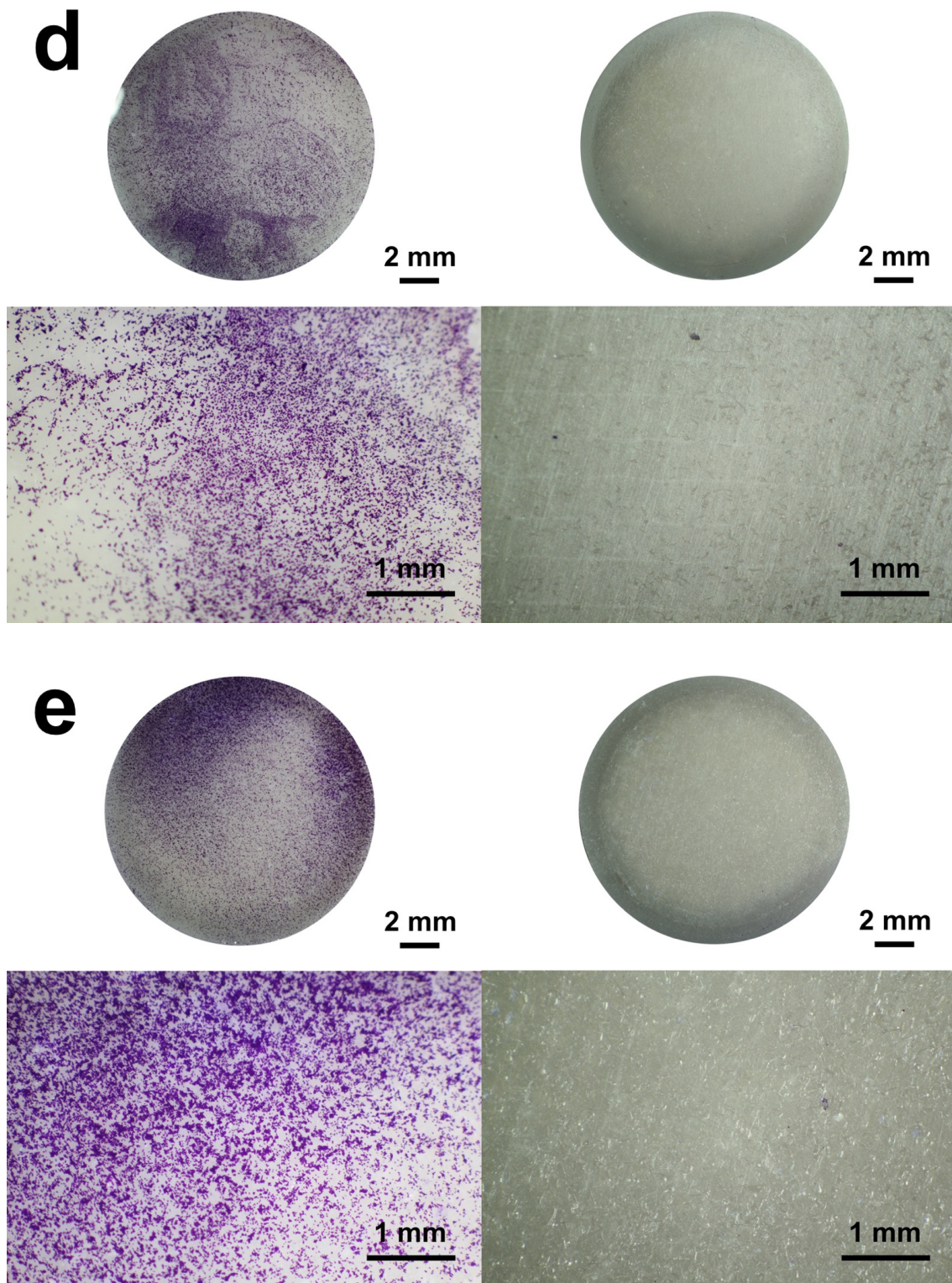


Figure 11 Optical micrographs of initial cell adhesion on experimental and control sample surfaces after four-hour cultivation stained by crystal violet at 7 $\times$  and 32 $\times$  magnification. (a) directly printed PEEK; (b) polished PEEK; (c) 50  $\mu\text{m}$   $\text{Al}_2\text{O}_3$  particle grit-blasted PEEK; (d) 120  $\mu\text{m}$   $\text{Al}_2\text{O}_3$  particle grit-blasted PEEK; (e) 250  $\mu\text{m}$   $\text{Al}_2\text{O}_3$  particle grit-blasted PEEK [25].

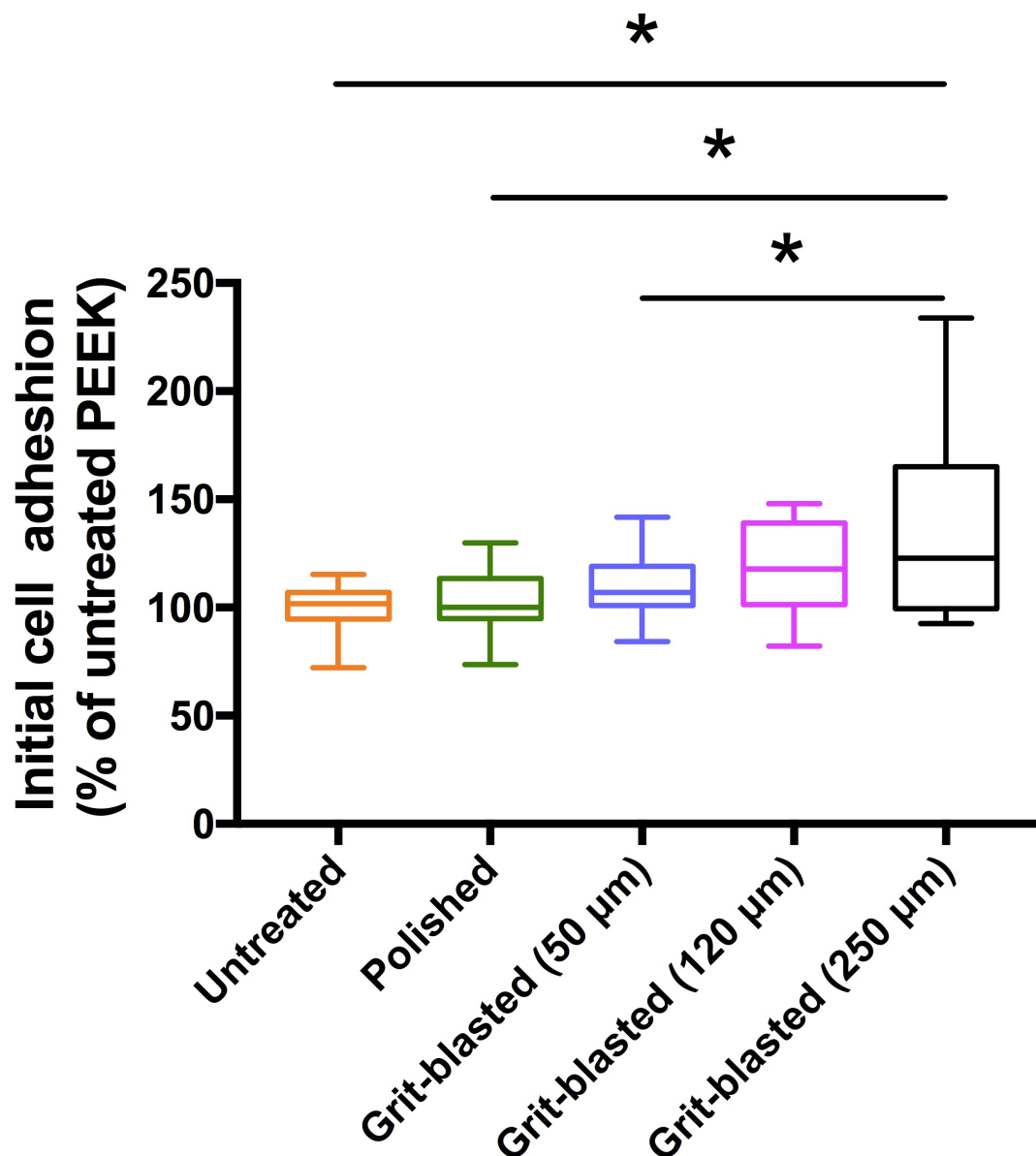


Figure 12 Initial cell adhesion of SAOS-2 osteoblasts stained with crystal violet after four hours. The untreated PEEK was considered to be the reference group (100%). \*  $p < 0.05$ .

### 3.2.2 Cell metabolic activity and proliferation

To analyze the influence of FFF printing structures and surface roughness on the growth of human osteoblasts, the CCK-8 assay was used to examine cell metabolic activity and as indirect evidence of cell proliferation. Table 6 and

### 3. Results

Figure 13 show the OD value of different groups (untreated, polished, 50  $\mu\text{m}$ , 120  $\mu\text{m}$ , and 250  $\mu\text{m}$   $\text{Al}_2\text{O}_3$  grit-blasted groups) at different time points (1st day, 3rd day, and 5th day). Results indicated that after 1-day incubation, there was no obvious difference among untreated, polished, and grit-blasted groups. The CCK-8 reduction activity of SAOS-2 osteoblasts on untreated sample surfaces increased slightly further compared with the other groups. As the culturing time increased, the differences became more obvious. After incubation for three days, the directly printed groups indicated a significant higher OD value, which was a two-fold or three-fold increase of cell metabolic activity in comparison to the other four groups. The OD values after five days' incubation indicated a similar trend as observed with the three days' results that the untreated group represented a significantly higher cell metabolic activity compared with other groups. Besides, the differences among the three grit-blasted groups were not significant ( $p > 0.05$ ), and the proliferation of osteoblasts cultivated on polished surfaces was significantly higher than the three grit-blasted groups after three and five days.

Table 6 The OD values (means  $\pm$  standard deviations) of cell proliferation test.

Group	Day 1	Day 3	Day 5
Untreated	0.69 $\pm$ 0.07 <sup>a</sup>	1.57 $\pm$ .021 <sup>a</sup>	2.50 $\pm$ 0.42 <sup>a</sup>
Polished	0.50 $\pm$ 0.05 <sup>b</sup>	0.76 $\pm$ 0.23 <sup>b</sup>	1.36 $\pm$ 0.46 <sup>b</sup>
Grit-blasted (50 $\mu\text{m}$ )	0.59 $\pm$ 0.12 <sup>c</sup>	0.59 $\pm$ 0.12 <sup>c</sup>	1.00 $\pm$ 0.95 <sup>c</sup>
Grit-blasted (120 $\mu\text{m}$ )	0.48 $\pm$ 0.10 <sup>b</sup>	0.60 $\pm$ 0.07 <sup>c</sup>	0.85 $\pm$ 0.14 <sup>c</sup>
Grit-blasted (250 $\mu\text{m}$ )	0.59 $\pm$ 0.14 <sup>c</sup>	0.65 $\pm$ 0.06 <sup>c</sup>	0.90 $\pm$ 0.14 <sup>c</sup>

Different lowercase letters in the same column indicate significantly different groups ( $p < 0.05$ ).

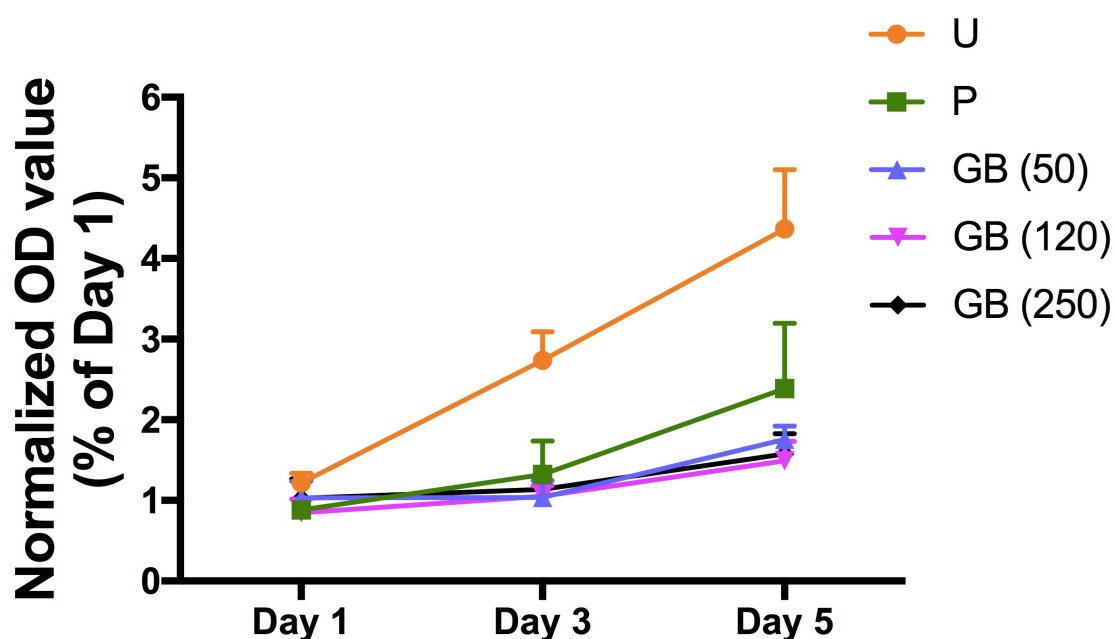
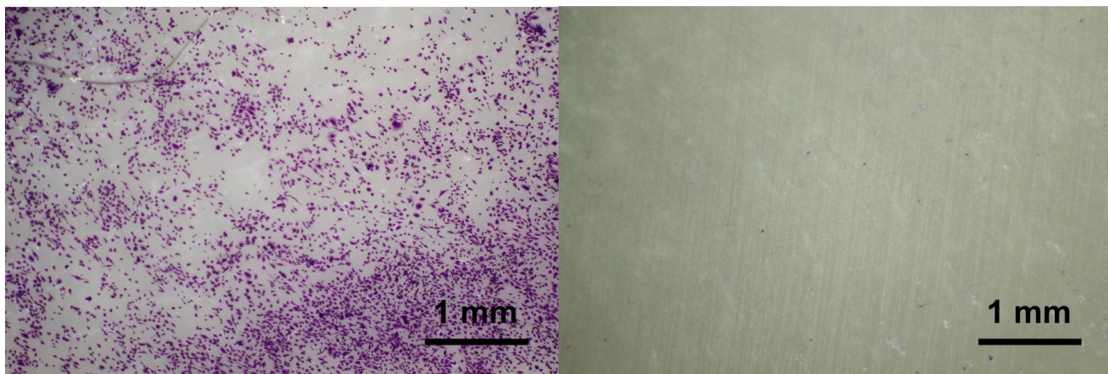
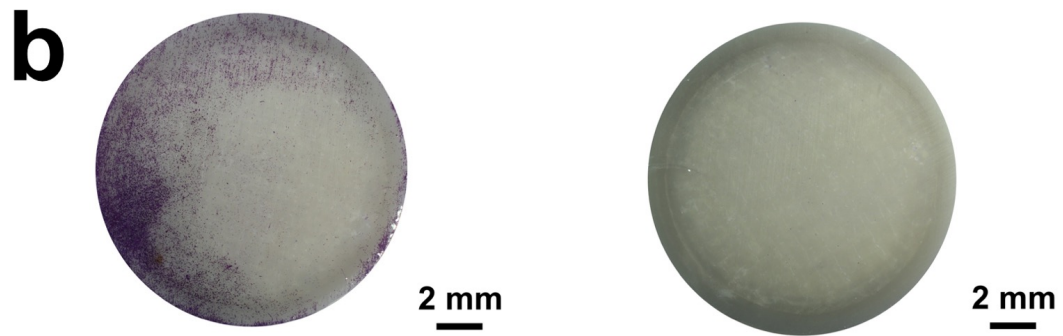
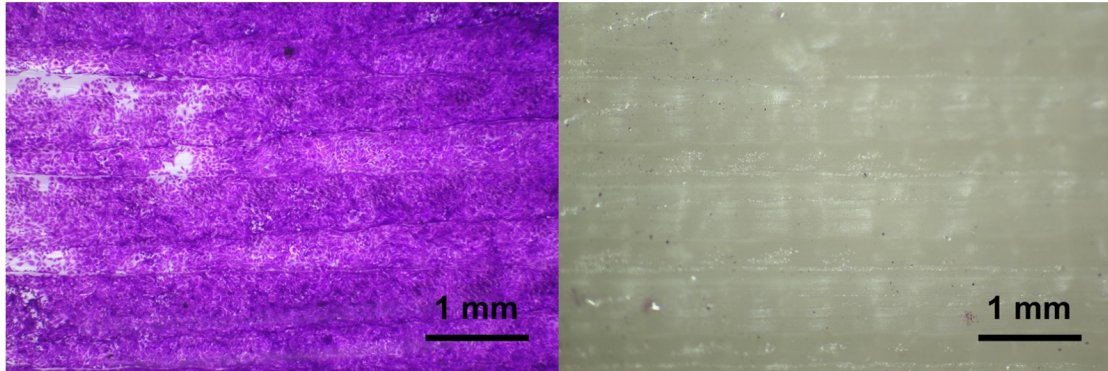
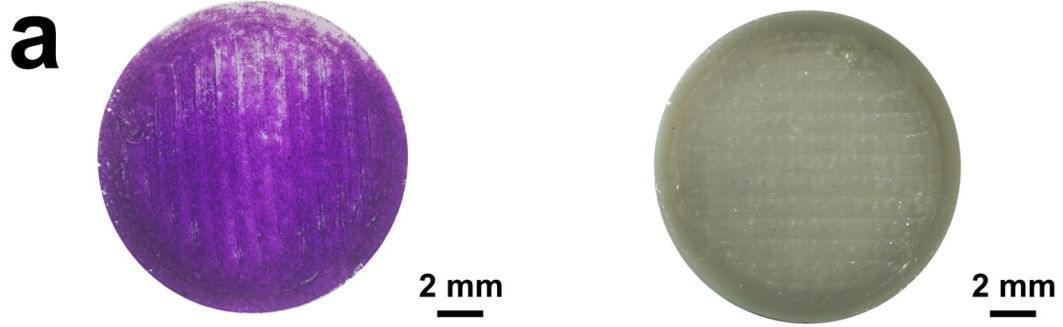


Figure 13 Cell metabolic activity and proliferation test of SAOS-2 osteoblasts tested by CCK-8 assay of different groups at different time points. The data are presented as means  $\pm$  standard deviations. U: untreated group; P: polished group; GB (50): 50  $\mu\text{m}$  grit-blasted group; GB (120): 120  $\mu\text{m}$  grit-blasted group; GB (250): 250  $\mu\text{m}$  grit-blasted group [25].

### 3.2.3 Sample surface coverage

Cell coverage on the sample surfaces in different groups was measured five days after seeding, stained by crystal violet dye. Figure 14 and 17 indicated the optical micrographs of the sample surfaces and the quantitative result of surface coverage by osteoblasts. Data showed that after incubation for five days, the untreated PEEK sample surfaces led to the highest surface coverage by SAOS-2 osteoblast cells (100%). Cell coverage was significantly lower on polished samples (30%) and the three grit-blasted groups (50  $\mu\text{m}$  grit-blasted group: 18%, 120  $\mu\text{m}$  grit-blasted group: 13%, and 250  $\mu\text{m}$  grit-blasted group: 12%). Besides, the cell surface coverage of the polished samples was higher compared with the grit-blasted samples ( $p < 0.05$ ), and the differences between the three grit-blasted groups were not statistically significant.







### 3. Results

---

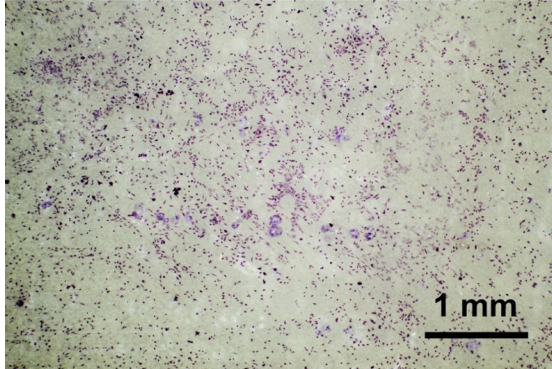
**c**



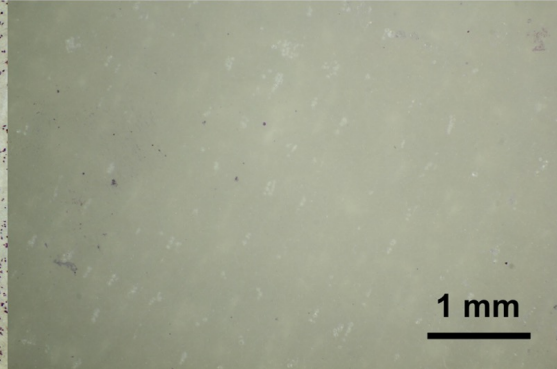
2 mm



2 mm

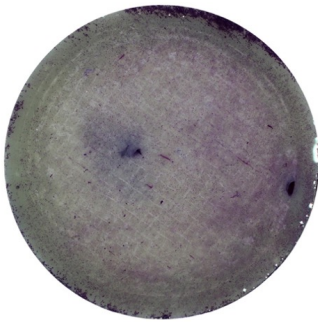


1 mm



1 mm

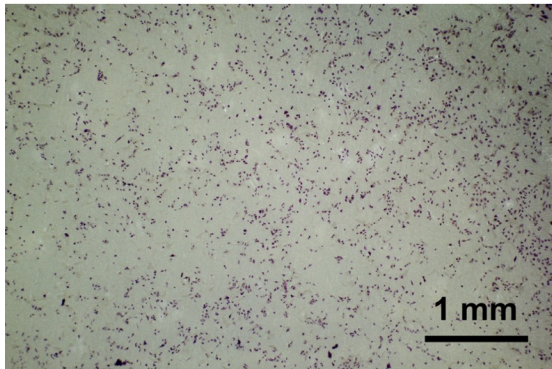
**d**



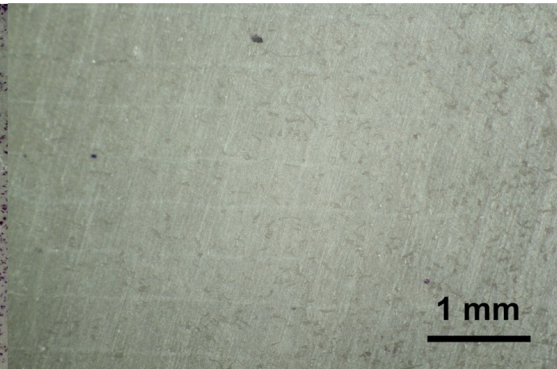
2 mm



2 mm



1 mm



1 mm

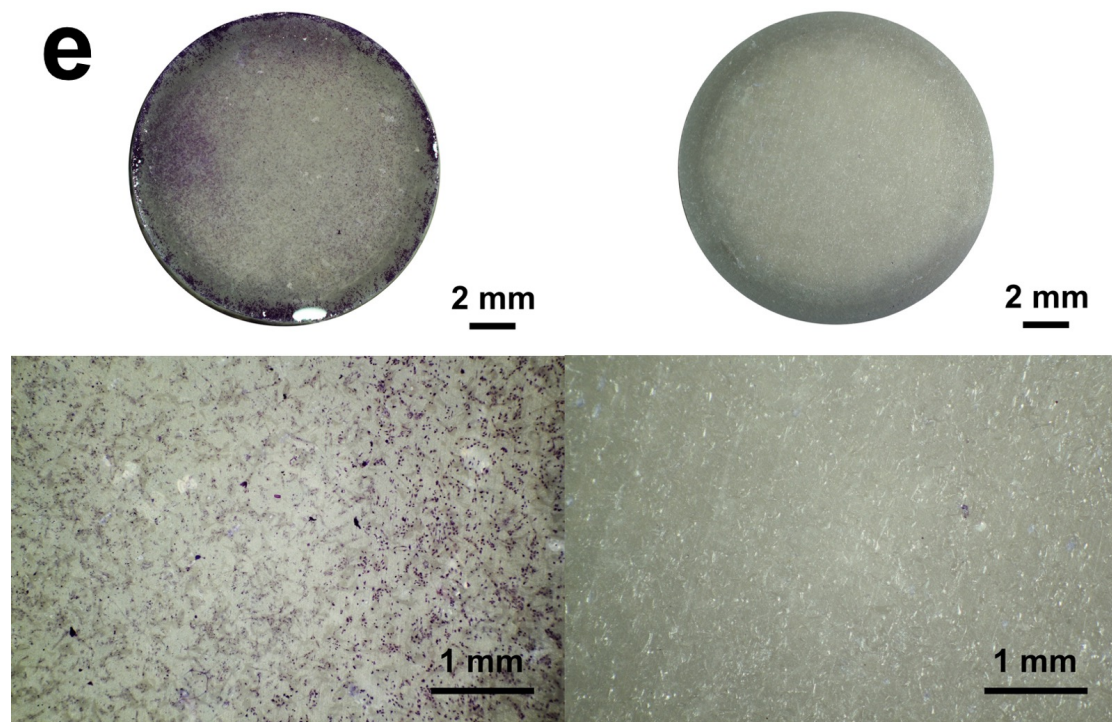


Figure 14 Optical micrographs of surface coverage of SAOS-2 osteoblasts after incubation for five days stained with crystal violet of experimental and control groups at 7 $\times$  and 32 $\times$  magnification. (a) directly printed PEEK; (b) polished PEEK; (c) 50  $\mu\text{m}$   $\text{Al}_2\text{O}_3$  particle grit-blasted PEEK; (d) 120  $\mu\text{m}$   $\text{Al}_2\text{O}_3$  particle grit-blasted PEEK; (e) 250  $\mu\text{m}$   $\text{Al}_2\text{O}_3$  particle grit-blasted PEEK.

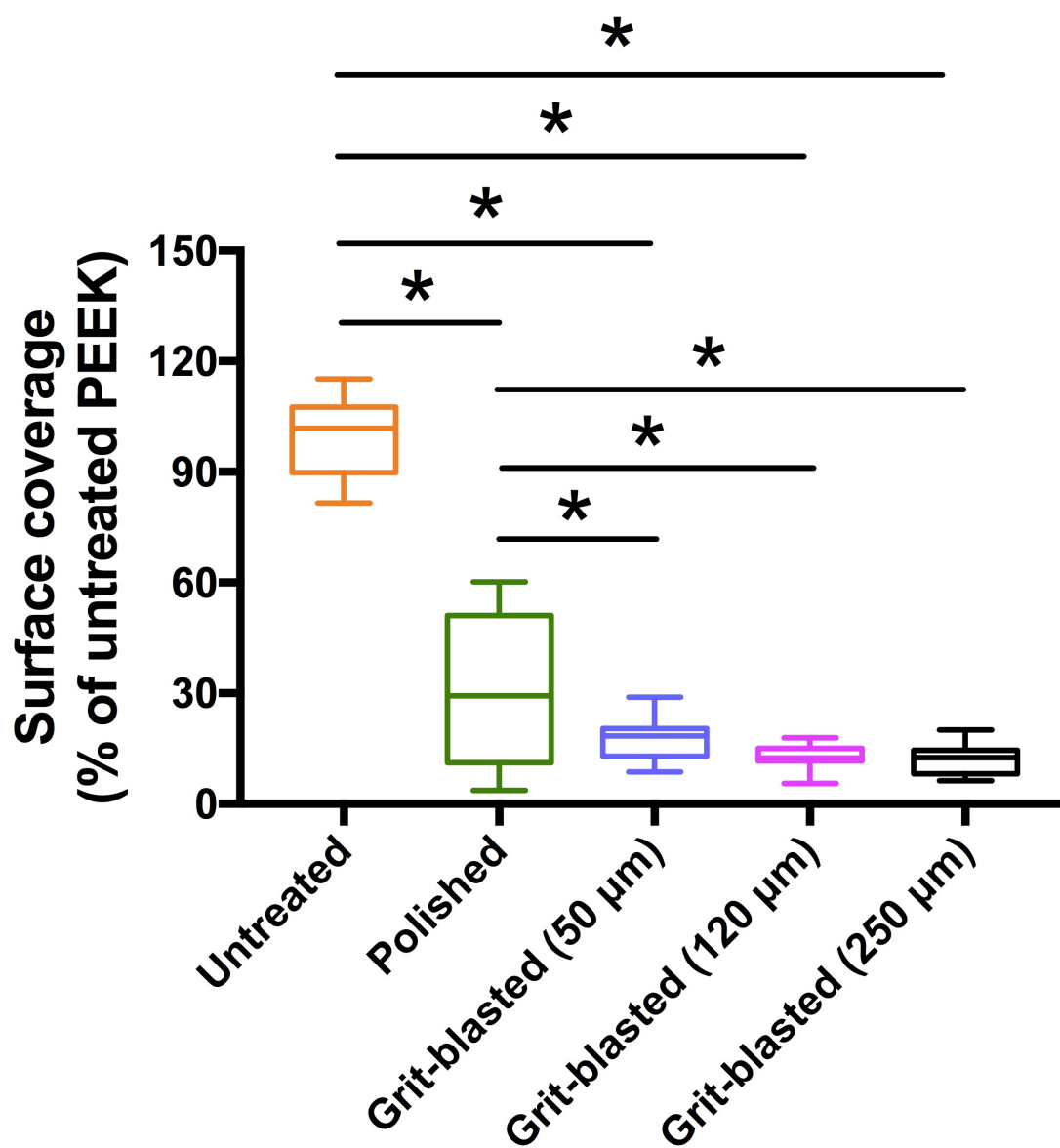


Figure 15 Surface coverage of SAOS-2 after incubation for five days stained with crystal violet. \*  $p < 0.05$ .

### 4 Discussion

PEEK has been widely used in the medical fields during the past decades, e.g., dental implants, cranioplasty, joint replacements, interbody fusion, and cardiac surgery [92]. From the biomedical perspective, PEEK has excellent cell biocompatibility and corrosion resistance. Besides, the mechanical strength of PEEK is close to those of human bones [3]. In some previous papers, the biocompatibility, crystallinity, and mechanical properties of FFF-printed PEEK have been studied [3,24,25,87]. However, studies about the bioactivities of the FFF-printed PEEK still lack, like cell adhesion, metabolic activity, proliferation, and long-term cell coverage. In this study, the bioactivities of FFF-printed PEEK have been analyzed systematically.

Polishing and grit-blasting are two common mechanical surface treatments to get smooth or rough surfaces. In this study, the FFF-printed PEEK samples were modified by polishing and grit-blasting methods to obtain different surface morphology and roughness. The microstructure and roughness results indicated that the untreated samples represented a significantly higher surface roughness compared to the polished and grit-blasted groups with distinct printing peaks and valleys on the surfaces (Figure 8 and Figure 9). The reason for the highly roughened surface and unique features of the directly printed group might be due to the working principle of the FFF technology. When printing an FFF object, the thermoplastic materials are extruded from the nozzle to form a 2D layer [82]. The final model is constructed by melting the layers together. During this printing procedure, the unfilled areas could appear between lines and layer, which builds the unique printing structures on the sample surfaces [93].

After polishing, the FFF printing structures were obliterated, and the surface roughness reduced dramatically. The grit-blasted groups showed a slightly



higher roughened surface compared with the polished group, and the roughness value increased with the rise of  $Al_2O_3$  particles. However, the difference in roughness values between the polished and grit-blasted groups was not very obvious compared with some previous studies, within the interval of 0.17-0.52  $\mu m$  [94,95]. This is because, in this study, the PEEK samples were FFF printed with a layer thickness of 200  $\mu m$ . If higher grit-blasted parameters were applied, the upper surface might be destroyed and exfoliated. As shown in Figure 16, if a high pressure, a long time or a short distance were applied, the first layer would be damaged [3]. Thus, because of the grit-blasting parameters chosen in this research, the grit-blasted groups indicated slightly higher roughness values than the polished group.

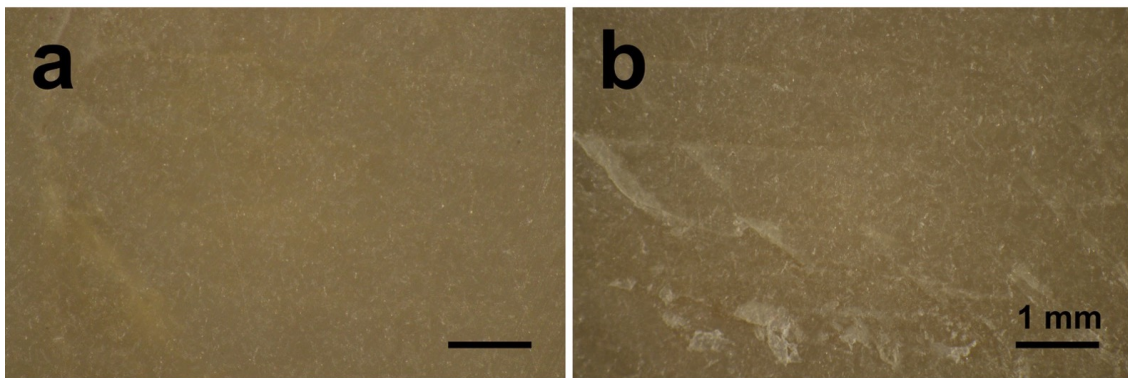


Figure 16 Optical micrographs of grit-blasted PEEK samples under different grit-blasting parameters: (a) distance: 50 mm, pressure: 0.1 MPa, time: 15 s; (b) distance: 50 mm, pressure: 0.5 MPa, time: 15 s [3].

Normally, surfaces with high hydrophilicity could improve the initial cell reactions on implant surfaces, which is also benefited to bone healing and osseointegration [96]. Surface wettability could affect the biological system in four aspects: (i) proteins and other macromolecules' adhesion onto the surface (conditioning); (ii) cell interactions of hard and soft tissue with the preconditioned surfaces; (iii) adhesion of bacteria and biofilm formation; and (iv) in vivo

osseointegration [97]. In this study, the difference in water contact angle among different groups was not significant (Figure 10). This result indicated that, based on the materials and parameters of polishing and grit-blasting in this study, these two surface treatments methods didn't have a big influence on sample surface wettability.

Usually, the low or highly roughened surfaces are not suitable for the water droplets to spread. This is because the peaks and valleys on smooth surfaces are not sufficient for droplet spreading. However, the huge peaks and valleys on highly roughened surfaces, might be the "geometrical barriers" and hinder the droplet from spreading on sample surfaces [94,98]. This might be the reason why there was not a big difference in hydrophilicity before and after surface treatments. In this study, the untreated PEEK surfaces were highly roughened ( $R_a = 22.28 \mu\text{m}$ ) with particular printing structures. The printing structures might be the "geometrical barriers" to prevent water from spreading [98]. And for the polished and grit-blasted groups, the surface roughness was similar with a  $R_a$  value range of  $0.17\text{-}0.52 \mu\text{m}$ , which were not ideal for water to spread, either. Elawadly et al. compared the surface roughness and wettability of PEEK samples and found that within a certain interval, higher surface roughness leads to a lower contact angle of PEEK [99]. Moreover, the wettability decreased when the  $R_a$  values are either below  $1\mu\text{m}$  or above  $1.7\mu\text{m}$ . This finding is in accord with our result.

Better initial cell adhesion might induce more bone tissue around the scaffold [100]. In this study, the initial cell adhesion of the SAOS-2 osteoblasts was measured after 4 hours, which was considered to be the "decisive period" for cell attachment in the early stage [95]. The result showed that the surface coverage by SAOS-2 osteoblast cells in different groups were quite similar after four hours,

except for the 250  $\mu\text{m}$  grit-blasted group (Figure 11 and Figure 12). This finding was consistent with the wettability result, although the surface roughness was different between the untreated group and the other groups. This indicated that compared with surface roughness, surface wettability plays a more important role in the initial cell adhesion stage. Ranella et al. studied the fibroblast attachment and metabolic activity on silicon material surfaces with gradient roughness ratios and wettability and found that surface wettability could influence cell reactions [101]. Huang et al. also analyzed a possible relation between sample surface wettability and the adhesion of different cells. They found that hydrophobicity could inhibit cell attachment and spreading, while on the hydrophilic regions, enhanced cell attachment could be observed [102]. In our study, the contact angle of all samples was close to  $90^\circ$  and supported initial cell adhesion in general, respectively. The similar cell attachment in the early stage might be due to the similar surface hydrophilicity.

To evaluate the long-term cell responses on different surface morphology and roughness of FFF-printed sample surfaces, cell metabolic activity and proliferation were also probed after one day, three days, and five days by CCK-8 assay. As shown in Figure 13, after one day, SAOS-2 cells grew rapidly on the highly roughened surfaces (untreated group), with a proliferation rate higher than the polished and grit-blasted groups. While after three days and five days, the cell metabolic activity on the untreated surfaces was significantly higher compared with others ( $\approx 2 - 3$  times). This result in accord with some previous research suggesting that rough structures are proper for cell metabolic activity and proliferation compared with smooth surfaces [41,42]. A possible explanation for the directly printed surfaces having a beneficial effect on cell viability is the unique FFF printing structures and high surface roughness.

Usually, the high roughness produced by FFF is thought to be a significant drawback of this technique [103]. For some engineering models, some post-processing processes are needed to eliminate or modify the surfaces [104]. However, to improve the cell metabolic activity and proliferation, the roughness produced by FFF is beneficial. The unique printing topography cannot be achieved by the dental grit-blasting method. Usually, a larger surface area available, a more cell interaction would arise [105]. The large surface allows for cell attachment, anchorage, growth, migration, and proliferation. Similar to an earlier study, with the extension of culturing time, untreated sample surfaces with extended surface area represented significantly improved cell proliferation rate due to more spaces for cells to attach and spread [3]. Besides, the particular FFF printing structures may also contribute to the increased cell metabolic activity and proliferation (Figure 8a and Figure 9a) [3]. The cells might slide into the grooves produced by FFF printing process, and the cells were not easily detached by later experimental steps. Figure 17 indicated the cell attachment of L929 fibroblasts after 24 hours culturing, which shows that the cells were attached not on a flat surface, and they adhered on different surface height [3]. Moreover, apparent cell accumulation in the grooves resulting from FFF manufacturing process could be observed.

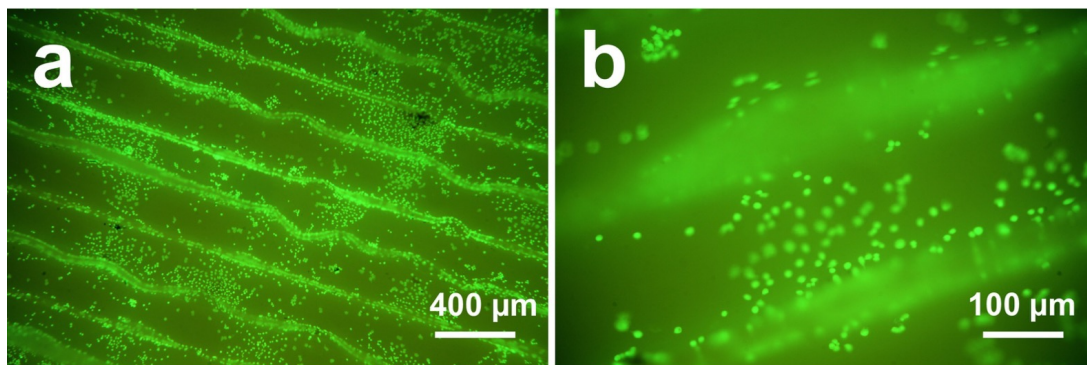


Figure 17 LIVE/DEAD staining of L929 fibroblast cell attachment on PEEK



sample surfaces after culturing for 24 h at different magnifications: (a) 25 × magnification; (b) 100 × magnification [3].

As a final test, an investigation of cell coverage on sample surfaces was performed after five days of incubation by crystal violet staining. This measurement was chosen because it provides an alternative method to analyze cell density in both qualitative and quantitative assessments on different sample surfaces. The cell density observed on the untreated sample surfaces was much higher compared with the other groups (Figure 14 and Figure 15), which was in accord with the outcome of the CCK-8 assay.

Besides, the polished group indicated slightly higher OD values than the grit-blasted samples, and there was not an apparent difference in grit-blasted groups. This might be due to the residual  $\text{Al}_2\text{O}_3$  particles of grit-blasted groups. After grit-blasting, although the samples were cleaned and disinfected ultrasonically with DI water and ethanol, there might be still some  $\text{Al}_2\text{O}_3$  particles left on the sample surfaces [25,106]. The presence of alumina particles might influence cell spreading and impair cell metabolic activity and proliferation [106]. Rosales-Leal evaluated the effect of roughness, morphology, and wettability on cell adhesion of titanium surfaces and also found that residual alumina particles hindering cell spreading and proliferation as expected [107].

This study focused on different surface morphology and roughness of FFF-printed PEEK on bioactivities, including cell adhesion, metabolic activity, and proliferation. The results indicated that FFF technology is a potential candidate for manufacturing clinical PEEK objects, like orthopedic and dental implants.

As a consequence, similar to findings in our earlier study of PEEK, this in vitro

#### 4. Discussion

---

tests indicated that the FFF 3D-printed PEEK objects with optimal printing structures and surface roughness possess superior ability for cell adhesion, metabolic activity, and proliferation, which could be a potential candidate for the application in orthopedic and dental implants [3]. Besides, the results also showed that surface modification methods such as polishing and sandblasting could not improve the bioactivity of FFF 3D-printed PEEK, further studies should be focused on other surface treatment methods, like neutral atom beam or plasma techniques [45,58,106].

### 5 Summary

PEEK has been used widely in clinical applications during the past decades due to the excellent biocompatibility, low density, chemical resistance, radiolucency, and mechanical strength resembling human bone. As one of the fastest growing and most popular AM technologies, recently FFF has become a possible way to fabricate patient-specific PEEK objects to reconstruct severe bone loss. But to the best of our knowledge, studies focusing on the bioactivities of FFF-printed PEEK, e.g., cell adhesion, metabolic activity, and proliferation, are still lacking. Therefore, the aim of this study is to evaluate the effect of the specific FFF printing structure and surface morphology on cell adhesion, metabolic activity, and proliferation of SAOS-2 osteoblasts.

The PEEK disk samples were successfully manufactured by an FFF printer using medical grade PEEK filament with a layer thickness of 200  $\mu\text{m}$ . Then the sample surfaces were modified by polishing and by grit-blasting to obtain increased surface roughness [25]. Cell metabolic activity and proliferation were analyzed by CCK-8 assay after culturing for one day, three days, and five days. After five days, as a final test, the sample surface coverage of osteoblasts was measured by crystal violet again.

The result indicated that the FFF printed PEEK with particular printing structures and high roughness had improved bioactivity compared with polished and grit-blasted surfaces, especially in cell metabolic activity, proliferation, and long-term cell adhesion [25]. FFF printing features had an enlarged surface area, which could provide more bonding spots for cells to spread and migrate, which were beneficial to cell metabolic activity and proliferation. In the early stage of cell adhesion, surface wettability played an important role. While as the culture

time extent, the influence of the surface morphology and roughness became increasingly apparent.

FFF-manufactured samples have highly rough and unique printing topographies, which cannot be achieved by dental grit-blasting processes. These manufacturing features are more suitable for cell attachment, metabolic activity, and proliferation than the polished or grit-blasted surfaces. Therefore, based on the limitations of this research, FFF-printed PEEK could have great potential in bone reconstruction and replacement in oral and cranio-maxillofacial surgeries.

### 6 Zusammenfassung

PEEK wurde in den letzten Jahrzehnten aufgrund seiner hervorragenden Biokompatibilität, niedrigen Dichte, chemischen Beständigkeit, Radioluzenz und mechanischen Festigkeit, die dem menschlichen Knochen ähnelt, in klinischen Anwendungen eingesetzt. Als eine der am schnellsten wachsenden und beliebtesten AM-Technologien ist die FFF in jüngster Zeit eine Möglichkeit geworden, patientenspezifische PEEK-Objekte zur Rekonstruktion eines schweren Knochenverlusts herzustellen. Allerdings liegen noch keine Studien über die Bioaktivität von mit FFF gedrucktem PEEK vor. Daher zielt diese Studie darauf ab, den Einfluss der FFF-Druckstruktur und der Oberflächenmorphologie auf Zelladhäsion, Stoffwechselaktivität und Proliferation von SAOS-2-Osteoblasten zu bewerten.

Die PEEK-Plattenproben wurden mit einem FFF-Drucker unter Verwendung eines PEEK-Filaments mit einer Schichtdicke von 200 µm hergestellt. Dann wurden die Probenoberflächen durch Polieren und Sandstrahlen modifiziert, um eine erhöhte Oberflächenrauheit zu erhalten. Die anfängliche SAOS-2-Osteoblastenadhäsion wurde nach vierstündiger Inkubation mit einem Kristallviolettfarbstoff gemessen. Zellstoffwechselaktivität und Zellproliferation wurden nach einem drei und fünf Tagen mit dem CCK-8-Assay analysiert. Nach fünf Tagen wurde als abschließender Test die Bedeckung der Probenoberflächen mit Osteoblasten erneut mit Kristallviolett analysiert.

Das Ergebnis zeigte, dass das mit FFF bedruckte PEEK eine verbesserte Bioaktivität im Vergleich zu polierten und sandgestrahlten Oberflächen hatte, insbesondere in Bezug auf Zellstoffwechselaktivität, Proliferation und langfristige Zelladhäsion. FFF-gedruckte -Oberflächen hatten eine vergrößerte Oberfläche, die mehr Bindungspunkte für die Ausbreitung und Migration der Zellen

bereitstellen könnte, was für die Zellstoffwechselaktivität und die Zellproliferation von Vorteil wäre. Im frühen Stadium der Zelladhäsion spielte die Benetzbarkeit der Oberfläche eine wichtige Rolle. Mit zunehmender Zellkulturdauer wurde der Einfluss der Oberflächenmorphologie und der Rauheit deutlich.

FFF-gefertigte Proben weisen sehr raue und einzigartige gedruckte Topographien auf, die durch zahnärztliche Sandstrahlverfahren nicht erhalten werden können. Diese eignen sich besser für Zellanhaftung, Stoffwechselaktivität und Proliferation als die polierten oder sandgestrahlten Oberflächen. Daher bietet das mit FFF gedruckte PEEK mit seinen gedruckten Oberflächenfeaturesein großes Potential als Kandidat für orthopädische oder zahnärztliche Implantate in der Knochenreparatur, -regeneration oder beim Tissue Engineering.

## 7 References

- [1] Z.H. Ren, H.J. Wu, H.Y. Tan, K. Wang, S. Zhang, Transfer of anterolateral thigh flaps in elderly oral cancer patients: Complications in oral and maxillofacial reconstruction, *J. Oral Maxillofac. Surg.* 73 (2015) 534–540.
- [2] D. Rohner, R. Guijarro-Martínez, P. Bucher, B. Hammer, Importance of patient-specific intraoperative guides in complex maxillofacial reconstruction, *J. Cranio-Maxillofacial Surg.* 41 (2013) 382–390.
- [3] X. Han, D. Yang, C. Yang, S. Spintzyk, L. Scheideler, P. Li, D. Li, J. Geis-Gerstorfer, F. Rupp, Carbon Fiber Reinforced PEEK Composites Based on 3D-Printing Technology for Orthopedic and Dental Applications, *J. Clin. Med.* 8 (2019) 240.
- [4] M. Artico, L. Ferrante, F.S. Pastore, E.O. Ramundo, D. Cantarelli, D. Scopelliti, G. Iannetti, Bone autografting of the calvaria and craniofacial skeleton: Historical background, surgical results in a series of 15 patients, and review of the literature, *Surg. Neurol.* 60 (2003) 71–79.
- [5] B.L. Eppley, W.S. Pietrzak, M.W. Blanton, Allograft and Alloplastic Bone Substitutes: A Review of Science and Technology For the Craniomaxillofacial Surgeon, *J. Craniofac. Surg.* 16 (2005) 981–989.
- [6] T.W. Bauer, G.F. Muschler, Bone Graft Materials: An Overview of the Basic Science, *Clin. Orthop. Relat. Res.* 371 (2000) 10–27.
- [7] J. Torres, F. Tamimi, M. Alkhraisat, J. C. Prados-Frutos, E. Lopez-Cabarcos., Chapter 4 Bone Substitutes, 2011.
- [8] P. Tessier, H. Kawamoto, D. Matthews, J. Posnick, Y. Raulo, J.F. Tulasne, S.A. Wolfe, Autogenous Bone Grafts and Bone Substitutes — Tools and Techniques : I . A 20,000-Case Experience in Maxillofacial and Craniofacial Surgery, *Plast Reconstr Surg.* 116 (2005) 6–24.
- [9] M. Hallman, A. Thor, Bone substitutes and growth factors as an

## 7. References

---

- alternative/complement to autogenous bone for grafting in implant dentistry, *Periodontol.* 2000. 47 (2008) 172–192.
- [10] D.A. Harris, A.J. Fong, E.P. Buchanan, L. Monson, D. Khechoyan, S. Lam, History of synthetic materials in alloplastic cranioplasty, *Neurosurg. Focus.* 36 (2014) E20.
- [11] S. Stevenson, X.Q. Li, B. Martin, The fate of cancellous and cortical bone after transplantation of fresh and frozen tissue-antigen-matched and mismatched osteochondral allografts in dogs., *J. Bone Joint Surg. Am.* 73 (1991) 1143–1156.
- [12] J.F. Welter, J.W. Shaffer, S. Stevenson, D.T. Davy, G.A. Field, L. Klein, X.Q. Li, J.M. Zika, V.M. Goldberg, Cyclosporin A and tissue antigen matching in bone transplantation: fibular allografts studied in the dog, *Acta Orthop. Scand.* 61 (1990) 517–527.
- [13] J.J. Rodrigo, A.M. Schnaser, Jr.H.M. Reynolds, J.M. 3<sup>rd</sup>. Biggart, M.W. Leathers, S.E. Chism, E. Thorson, T. Grotz, Q.M. Yang, Inhibition of the immune response to experimental fresh osteoarticular allografts., *Clin. Orthop. Relat. Res.* (1989) 235–253.
- [14] H. Plenk, K. Hollmann, K.-H. Wilfert, Experimental bridging of osseous defects in rats by the implantation of Kiel bone containing fresh autologous marrow, *J. Bone Joint Surg. Br.* 54 (1972) 735–743.
- [15] S. Kobayashi, H. Hara, H. Okudera, T. Takemae, K. Sugita, Usefulness of Ceramic Implants in Neurosurgery, *Neurosurgery.* 21 (1987) 751–755.
- [16] S.H. Choi, M.L. Levy, J.G. McComb, A Method of Cranioplasty Using Coralline Hydroxyapatite, *Pediatr. Neurosurg.* 29 (1998) 324–327.
- [17] L.J. Smith, J.S. Swaim, C. Yao, K.M. Haberstroh, E.A. Nauman, T.J. Webster, Increased osteoblast cell density on nanostructured PLGA-coated nanostructured titanium for orthopedic applications., *Int. J. Nanomedicine.* 2 (2007) 493–499.



## 7. References

---

- [18] Y. Zhao, S.M. Wong, H.M. Wong, S. Wu, T. Hu, K.W.K. Yeung, P.K. Chu, Effects of Carbon and Nitrogen Plasma Immersion Ion Implantation on In vitro and In vivo Biocompatibility of Titanium Alloy, *ACS Appl. Mater. Interfaces*. 5 (2013) 1510–1516.
- [19] L. Wang, S. He, X. Wu, S. Liang, Z. Mu, J. Wei, F. Deng, Y. Deng, S. Wei, Biomaterials Polyetheretherketone / nano- fluorohydroxyapatite composite with antimicrobial activity and osseointegration properties, *Biomaterials*. 35 (2014) 6758–6775.
- [20] R. Ma, T. Tang, Current strategies to improve the bioactivity of PEEK, *Int. J. Mol. Sci*. 15 (2014) 5426–5445.
- [21] T. Kokubo, H.-M. Kim, M. Kawashita, Novel bioactive materials with different mechanical properties, *Biomaterials*. 24 (2003) 2161–2175.
- [22] S. Ramakrishna, J. Mayer, E. Wintermantel, K.W. Leong, Biomedical applications of polymer-composite materials: a review, *Compos. Sci. Technol*. 61 (2001) 1189–1224.
- [23] I.V. Panayotov, V. Orti, F. Cuisinier, J. Yachouh, Polyetheretherketone (PEEK) for medical applications, *J. Mater. Sci. Mater. Med*. 27 (2016) 118.
- [24] F. Zhao, D. Li, Z. Jin, Preliminary investigation of poly-ether-ether-ketone based on fused deposition modeling for medical applications, *Materials (Basel)*. 11 (2018) 288.
- [25] X. Han, N. Sharma, Z. Xu, L. Scheideler, J. Geis-Gerstorfer, F. Rupp, F.M. Thieringer, S. Spintzyk, An In Vitro Study of Osteoblast Response on Fused-Filament Fabrication 3D Printed PEEK for Dental and Cranio-Maxillofacial Implants, *J. Clin. Med*. 8 (2019) 771.
- [26] S.M. Kurtz, J.N. Devine, PEEK biomaterials in trauma, orthopedic, and spinal implants, *Biomaterials*. 28 (2007) 4845–4869.
- [27] S. Najeeb, M.S. Zafar, Z. Khurshid, F. Siddiqui, Applications of polyetheretherketone (PEEK) in oral implantology and prosthodontics, *J.*

- Prosthodont. Res. 60 (2016) 12–19.
- [28] S.J. Ferguson, J.M.A. Visser, A. Polikeit, The long-term mechanical integrity of non-reinforced PEEK-OPTIMA polymer for demanding spinal applications: experimental and finite-element analysis, *Eur. Spine J.* 15 (2006) 149–156.
- [29] V.A. Stadelmann, A. Terrier, D.P. Pioletti, Microstimulation at the bone–implant interface upregulates osteoclast activation pathways, *Bone.* 42 (2008) 358–364.
- [30] A. Godara, D. Raabe, S. Green, The influence of sterilization processes on the micromechanical properties of carbon fiber-reinforced PEEK composites for bone implant applications, *Acta Biomater.* 3 (2007) 209–220.
- [31] A.J. Barton, R.D. Sagers, W.G. Pitt, Bacterial adhesion to orthopedic implant polymers, *J. Biomed. Mater. Res. An Off. J. Soc. Biomater. Japanese Soc. Biomater.* 30 (1996) 403–410.
- [32] M.M. Kim, K.D.O. Boahene, P.J. Byrne, Use of customized polyetheretherketone (PEEK) implants in the reconstruction of complex maxillofacial defects, *Arch. Facial Plast. Surg.* 11 (2009) 53–57.
- [33] T.V. Thamaraiselvi, S. Rajeswari, Biological evaluation of bioceramic materials-a review, *Carbon N. Y.* 24 (2004) 172.
- [34] J.Y. Rho, R.B. Ashman, C.H. Turner, Young's modulus of trabecular and cortical bone material : Ultrasonic and microtensile measurements, *J. Biomech.* 26 (1993) 111–119.
- [35] W.-T. Lee, J.-Y. Koak, Y.-J. Lim, S.-K. Kim, H.-B. Kwon, M.-J. Kim, Stress shielding and fatigue limits of poly-ether-ether-ketone dental implants, *J. Biomed. Mater. Res. Part B Appl. Biomater.* 100 (2012) 1044–1052.
- [36] J. Sandler, P. Werner, M.S.P. Shaffer, V. Demchuk, V. Altstädt, A.H. Windle, Carbon-nanofibre-reinforced poly (ether ether ketone) composites,

- Compos. Part A Appl. Sci. Manuf. 33 (2002) 1033–1039.
- [37] M. Niinomi, Mechanical properties of biomedical titanium alloys, *Mater. Sci. Eng. A243*. 243 (1998) 231–236.
- [38] A. Rabiei, S. Sandukas, Processing and evaluation of bioactive coatings on polymeric implants, *J. Biomed. Mater. Res. Part A*. 101 (2013) 2621–2629.
- [39] T. Nieminen, I. Kallela, E. Wuolijoki, H. Kainulainen, I. Hiidenheimo, I. Rantala, Amorphous and crystalline polyetheretherketone: Mechanical properties and tissue reactions during a 3-year follow-up, *J. Biomed. Mater. Res. Part A*. 84 (2008) 377–383.
- [40] Y. Zheng, *Magnesium alloys as degradable biomaterials*, 2015.
- [41] R.A. Gittens, R. Olivares-navarrete, T. Mclachlan, Y. Cai, S.L. Hyzy, J.M. Schneider, Z. Schwartz, K.H. Sandhage, B.D. Boyan, Differential responses of osteoblast lineage cells to nanotopographically-modified, microroughened titanium–aluminum–vanadium alloy surfaces, *Biomaterials*. 33 (2012) 8986–8994.
- [42] W. Zhang, Z. Li, Q. Huang, L. Xu, J. Li, Y. Jin, G. Wang, X. Liu, X. Jiang, Effects of a hybrid micro / nanorod topography-modified titanium implant on adhesion and osteogenic differentiation in rat bone marrow mesenchymal stem cells, *Int. J. Nanomedicine*. 8 (2013) 257–265.
- [43] E. Occhiello, M. Morra, G.L. Guerrini, F. Garbassi, Adhesion properties of plasma-treated carbon/PEEK composites, *Composites*. 23 (1992) 193–200.
- [44] J. Waser-Althaus, A. Salamon, M. Waser, C. Padeste, M. Kreutzer, U. Pieves, B. Müller, K. Peters, Differentiation of human mesenchymal stem cells on plasma-treated polyetheretherketone, *J. Mater. Sci. Mater. Med*. 25 (2014) 515–525.
- [45] Z. Novotna, A. Reznickova, S. Rimpelova, M. Vesely, Z. Kolska, V. Svorcik, Tailoring of PEEK bioactivity for improved cell interaction: plasma

- treatment in action, *RSC Adv.* 5 (2015) 41428–41436.
- [46] F. Rupp, M. Haupt, H. Klostermann, H.-S. Kim, M. Eichler, A. Peetsch, L. Scheideler, C. Doering, C. Oehr, H.P. Wendel, S. Sinn, E. Decker, C. von Ohle, J. Geis-Gerstorfer, Multifunctional nature of UV-irradiated nanocrystalline anatase thin films for biomedical applications, *Acta Biomater.* 6 (2010) 4566–4577.
- [47] M. Miyauchi, A. Nakajima, T. Watanabe, K. Hashimoto, Photocatalysis and photoinduced hydrophilicity of various metal oxide thin films, *Chem. Mater.* 14 (2002) 2812–2816.
- [48] P. Zeman, S. Takabayashi, Effect of total and oxygen partial pressures on structure of photocatalytic TiO<sub>2</sub> films sputtered on unheated substrate, *Surf. Coatings Technol.* 153 (2002) 93–99.
- [49] R. Jimbo, D. Ono, Y. Hirakawa, T. Odatsu, T. Tanaka, T. Sawase, Accelerated photo-induced hydrophilicity promotes osseointegration: an animal study, *Clin. Implant Dent. Relat. Res.* 13 (2011) 79–85.
- [50] A. Funato, T. Ogawa, Photofunctionalized dental implants: a case series in compromised bone., *Int. J. Oral Maxillofac. Implants.* 28 (2013) 1589-1601.
- [51] K.-H. Park, J.-Y. Koak, S.-K. Kim, C.-H. Han, S.-J. Heo, The effect of ultraviolet-C irradiation via a bactericidal ultraviolet sterilizer on an anodized titanium implant: a study in rabbits., *Int. J. Oral Maxillofac. Implants.* 28 (2013) 57-66.
- [52] W. Att, N. Hori, F. Iwasa, M. Yamada, T. Ueno, T. Ogawa, The effect of UV-photofunctionalization on the time-related bioactivity of titanium and chromium–cobalt alloys, *Biomaterials.* 30 (2009) 4268–4276.
- [53] P. Laurens, B. Sadras, F. Decobert, F. Arefi-Khonsari, J. Amouroux, Enhancement of the adhesive bonding properties of PEEK by excimer laser treatment, *Int. J. Adhes. Adhes.* 18 (1998) 19–27.
- [54] A. Riveiro, R. Soto, R. Comesaña, M. Boutinguiza, J. del Val, F. Quintero, F.

- Lusquiños, J. Pou, Laser surface modification of PEEK, *Appl. Surf. Sci.* 258 (2012) 9437–9442.
- [55] M.S.A. Al Qahtani, Y. Wu, S. Spintzyk, P. Krieg, A. Killinger, E. Schweizer, I. Stephan, L. Scheideler, J. Geis-Gerstorfer, F. Rupp, UV-A and UV-C light induced hydrophilization of dental implants, *Dent. Mater.* 31 (2015) e157–e167.
- [56] R.K. Roeder, G.L. Converse, R.J. Kane, W. Yue, Hydroxyapatite-reinforced polymer biocomposites for synthetic bone substitutes, *Jom.* 60 (2008) 38–45.
- [57] S. Najeeb, Z. Khurshid, J.P. Matinlinna, F. Siddiqui, M.Z. Nassani, K. Baroudi, Nanomodified peek dental implants: Bioactive composites and surface modification - A review, *Int. J. Dent.* 2015 (2015).
- [58] H. Wang, T. Lu, F. Meng, H. Zhu, X. Liu, Enhanced osteoblast responses to poly ether ether ketone surface modified by water plasma immersion ion implantation, *Colloids Surfaces B Biointerfaces.* 117 (2014) 89–97.
- [59] M.S.A. Bakar, P. Cheang, K.A. Khor, Tensile properties and microstructural analysis of spheroidized hydroxyapatite–poly (etheretherketone) biocomposites, *Mater. Sci. Eng. A.* 345 (2003) 55–63.
- [60] G.L. Converse, W. Yue, R.K. Roeder, Processing and tensile properties of hydroxyapatite-whisker-reinforced polyetheretherketone, *Biomaterials.* 28 (2007) 927–935.
- [61] L. Wang, L. Weng, S. Song, Z. Zhang, S. Tian, R. Ma, Characterization of polyetheretherketone–hydroxyapatite nanocomposite materials, *Mater. Sci. Eng. A.* 528 (2011) 3689–3696.
- [62] P. Honigmann, N. Sharma, B. Okolo, U. Popp, B. Msallem, F.M. Thieringer, Patient-specific surgical implants made of 3D printed PEEK: Material, technology, and scope of surgical application, *Biomed Res. Int.* 2018 (2018).

## 7. References

---

- [63] R. van Noort, The future of dental devices is digital, *Dent. Mater.* 28 (2012) 3–12.
- [64] C. Schubert, M.C. van Langeveld, L.A. Donoso, Innovations in 3D printing: a 3D overview from optics to organs, *Br. J. Ophthalmol.* 98 (2014) 159 LP-161.
- [65] B. Mueller, Additive manufacturing technologies–Rapid prototyping to direct digital manufacturing, *Assem. Autom.* 32 (2012).
- [66] J. Banks, Adding value in additive manufacturing: Researchers in the United Kingdom and Europe look to 3D printing for customization, *IEEE Pulse.* 4 (2013) 22–26.
- [67] J.N. Fullerton, G.C.M. Frodsham, R.M. Day, 3D printing for the many, not the few, *Nat. Biotechnol.* 32 (2014) 1086.
- [68] M. Attaran, The rise of 3-D printing: The advantages of additive manufacturing over traditional manufacturing, *Bus. Horiz.* 60 (2017) 677–688.
- [69] D. Hoang, D. Perrault, M. Stevanovic, A. Ghiassi, Surgical applications of three-dimensional printing : A review of the current literature & how to get started, 4 (2016) 456.
- [70] H.H. Malik, A.R.J. Darwood, S. Shaunak, P. Kulatilake, A.A. El-hilly, O. Mulki, A. Baskaradas, Three-dimensional printing in surgery : A review of current surgical applications, *J. Surg. Res.* 199 (2015) 512–522.
- [71] P. Bartlett, L.M. Carter, J.L. Russell, The Leeds method for titanium cranioplasty construction, *Br. J. Oral Maxillofac. Surg.* 47 (2009) 238–240.
- [72] P.S.-H. Chang, T.H. Parker, C.W. Patrick, M.J. Miller, The accuracy of stereolithography in planning craniofacial bone replacement, *J. Craniofac. Surg.* 14 (2003) 164–170.
- [73] J.-Y. Choi, J.-H. Choi, N.-K. Kim, Y. Kim, J.-K. Lee, M.-K. Kim, J.-H. Lee, M.-J. Kim, Analysis of errors in medical rapid prototyping models, *Int. J.*

- Oral Maxillofac. Surg. 31 (2002) 23–32.
- [74] D.J. Jeanmonod, Rebecca, Clinical applications of rapid prototyping models in cranio-maxillofacial surgery, *Intech Open*. 2 (2018) 64.
- [75] J.W. Choi, N. Kim, Clinical application of three-dimensional printing technology in craniofacial plastic surgery, *Arch. Plast. Surg.* (2015) 267–277.
- [76] D.N. Silva, M.G. de Oliveira, E. Meurer, M.I. Meurer, J.V.L. da Silva, A. Santa-Bárbara, Dimensional error in selective laser sintering and 3D-printing of models for craniomaxillary anatomy reconstruction, *J. Cranio-Maxillofacial Surg.* 36 (2008) 443–449.
- [77] M. Schmidt, D. Pohle, T. Rechtenwald, Selective laser sintering of PEEK, *CIRP Ann. Technol.* 56 (2007) 205–208.
- [78] K.H. Tan, C.K. Chua, K.F. Leong, C.M. Cheah, W.S. Gui, W.S. Tan, F.E. Wiria, Selective laser sintering of biocompatible polymers for applications in tissue engineering, *Biomed. Mater. Eng.* 15 (2005) 113–124.
- [79] K.H. Tan, C.K. Chua, K.F. Leong, M.W. Naing, C.M. Cheah, Fabrication and characterization of three-dimensional poly(ether-ether-ketone)/-hydroxyapatite biocomposite scaffolds using laser sintering, *Proc. Inst. Mech. Eng. Part H J. Eng. Med.* 219 (2005) 183–194.
- [80] M. Yan, X. Tian, G. Peng, D. Li, X. Zhang, High temperature rheological behavior and sintering kinetics of CF/PEEK composites during selective laser sintering, *Compos. Sci. Technol.* 165 (2018) 140–147.
- [81] X. Deng, Z. Zeng, B. Peng, S. Yan, W. Ke, Mechanical properties optimization of poly-ether-ether-ketone via fused deposition modeling, *Materials (Basel)*. 11 (2018) 216.
- [82] Y. Xu, A. Unkovskiy, F. Klaue, F. Rupp, J. Geis-Gerstorfer, S. Spintzyk, Compatibility of a silicone impression/adhesive system to FDM-printed tray

- materials—a laboratory peel-off study, *Materials (Basel)*. 11 (2018) 1905.
- [83] R. Anitha, S. Arunachalam, P. Radhakrishnan, Critical parameters influencing the quality of prototypes in fused deposition modelling, *J. Mater. Process. Technol.* 118 (2001) 385–388.
- [84] W.Z. Wu, P. Geng, J. Zhao, Y. Zhang, D.W. Rosen, H.B. Zhang, Manufacture and thermal deformation analysis of semicrystalline polymer polyether ether ketone by 3D printing, *Mater. Res. Innov.* 18 (2014) S5-12.
- [85] D. Garcia-Gonzalez, A. Rusinek, T. Jankowiak, A. Arias, Mechanical impact behavior of polyether–ether–ketone (PEEK), *Compos. Struct.* 124 (2015) 88–99.
- [86] B. Valentan, Ž. Kadivnik, T. Brajljih, A. Anderson, I. Drstvenšek, Processing poly (ether etherketone) on a 3D printer for thermoplastic modelling, *Mater. Tehnol.* 47 (2013) 715–721.
- [87] C. Yang, X. Tian, D. Li, Y. Cao, F. Zhao, C. Shi, Influence of thermal processing conditions in 3D printing on the crystallinity and mechanical properties of PEEK material, *J. Mater. Process. Technol.* 248 (2017) 1–7.
- [88] I. Standard, International Standard ISO 16610-71: Geometrical product specifications (GPS) -- Filtration -- Part 71: Robust areal filters: Gaussian regression filters, 2014 (2014).
- [89] E.S. Gadelmawla, M.M. Koura, T.M.A. Maksoud, I.M. Elewa, H.H. Soliman, Roughness parameters, *J. Mater. Process. Technol.* 123 (2002) 133–145.
- [90] C. Faille, J.-M. Membre, J.-P. Ussier, M.-N. Bellon-Fontaine, B. Carpentier, M.-A. Laroche, T. Benezech, Influence of physicochemical properties on the hygienic status of stainless steel with various finishes, *Biofouling*. 15 (2000) 261–274.
- [91] L. Gurau, H. Mansfield-Williams, M. Irle, Filtering the roughness of a sanded wood surface, *Holz Als Roh- und Werkst.* 64 (2006) 363–371.
- [92] Y. Guo, S. Chen, J. Wang, B. Lu, Medical applications of polyether ether



- ketone, *Transl. Surg.* 3 (2018) 12.
- [93] I. Gajdoš, J. Slota, Influence of printing conditions on structure in FDM prototypes, *Teh. Vjesn.* 20 (2013) 231–236.
- [94] R. Ourahmoune, M. Salvia, T.G. Mathia, N. Mesrati, Surface morphology and wettability of sandblasted PEEK and its composites, *Scanning.* 36 (2014) 64–75.
- [95] Y. Deng, X. Liu, A. Xu, L. Wang, Z. Luo, Y. Zheng, F. Deng, J. Wei, Z. Tang, S. Wei, Effect of surface roughness on osteogenesis in vitro and osseointegration in vivo of carbon fiber-reinforced polyetheretherketone–Nanohydroxyapatite composite, *Int. J. Nanomedicine.* 10 (2015) 1425–1447.
- [96] F. Rupp, R.A. Gittens, L. Scheideler, A. Marmur, B.D. Boyan, Z. Schwartz, J. Geis-Gerstorfer, A review on the wettability of dental implant surfaces I: Theoretical and experimental aspects, *Acta Biomater.* 10 (2014) 2894–2906.
- [97] R.A. Gittens, L. Scheideler, F. Rupp, S.L. Hyzy, J. Geis-Gerstorfer, Z. Schwartz, B.D. Boyan, A review on the wettability of dental implant surfaces II: Biological and clinical aspects, *Acta Biomater.* 10 (2014) 2907–2918.
- [98] K.J. Kubiak, M.C.T. Wilson, T.G. Mathia, P. Carval, Wettability versus roughness of engineering surfaces, *Wear.* 271 (2011) 523–528.
- [99] T. Elawadly, I.A.W. Radi, A. El Khadem, Reham B. Osman, Can PEEK be an implant material ? Evaluation of surface topography and wettability of filled versus unfilled PEEK with different surface roughness, *J. Oral Implantol.* 43 (2017) 456–461.
- [100] Y. Zhao, H.M. Wong, W. Wang, P. Li, Z. Xu, E.Y.W. Chong, C.H. Yan, K.W.K. Yeung, P.K. Chu, Cytocompatibility, osseointegration, and bioactivity of three-dimensional porous and nanostructured network on

## 7. References

---

- polyetheretherketone, *Biomaterials*. 34 (2013) 9264–9277.
- [101] A. Ranella, M. Barberoglou, S. Bakogianni, C. Fotakis, E. Stratakis, Tuning cell adhesion by controlling the roughness and wettability of 3D micro/nano silicon structures, *Acta Biomater.* 6 (2010) 2711–2720.
- [102] Q. Huang, L. Lin, Y. Yang, R. Hu, E.A. Vogler, C. Lin, Role of trapped air in the formation of cell-and-protein micropatterns on superhydrophobic/superhydrophilic microtemplated surfaces, *Biomaterials*. 33 (2012) 8213–8220.
- [103] M.S. Alsoufi, A.E. Elsayed, How Surface Roughness Performance of Printed Parts Manufactured by Desktop FDM 3D Printer with PLA+ is Influenced by Measuring Direction, *Am. J. Mech. Eng.* 5 (2017) 211–222.
- [104] I.F. Ituarte, S. Chekurov, M. Salmi, J. Tuomi, J. Partanen, Post-processing opportunities of professional and consumer grade 3D printing equipment: a comparative study, *Int. J. Rapid Manuf.* 5 (2015) 58–75.
- [105] E. Carletti, A. Motta, C. Migliaresi, Scaffolds for tissue engineering and 3D cell culture, in: *3D Cell Cult.*, Springer (2011) 17–39.
- [106] J.I. Rosales-Leal, M.A. Rodríguez-Valverde, G. Mazzaglia, P.J. Ramón-Torregrosa, L. Díaz-Rodríguez, O. García-Martínez, M. Vallecillo-Capilla, C. Ruiz, M.A. Cabrerizo-Vílchez, Effect of roughness, wettability and morphology of engineered titanium surfaces on osteoblast-like cell adhesion, *Colloids Surfaces A Physicochem. Eng. Asp.* 365 (2010) 222–229.
- [107] K. Anselme, M. Bigerelle, B. Noel, E. Dufresne, D. Judas, A. Lost, P. Hardouin, Qualitative and quantitative study of human osteoblast adhesion on materials with various surface roughnesses, *J. Biomed. Mater. Res. An Off. J. Soc. Biomater. Japanese Soc. Biomater.* 49 (2000) 155–166.

## **Declaration of Contribution**

This study was performed in Section of Medical Material Science and Technology, University Hospital Tübingen under the supervision of Prof. Dr. Frank Rupp.

Prof. Dr. Jürgen Geis-Gerstorfer, Prof. Dr. Frank Rupp, Dr. Lutz Scheideler, and Mr. Sebastian Spintzyk were involved in the concepts and hypotheses. Prof. Dr. Frank Rupp has corrected the manuscript.

The Department of Medical Additive Manufacturing Research Group, Hightech Research Center, Department of Biomedical Engineering, University of Basel, Allschwil, Switzerland, has provided the FDM-printed PEEK samples. Dr. Florian M. Thieringer and Mrs. Neha Sharma have printed the PEEK samples by the FDM printer.

Mr. Ernst Schweizer has provided the SEM images. Mr. Sebastian Spintzyk was involved in the surface modifications of polishing and grit-blasting, and roughness measurements. Ms. Ingrid Stephan and Ms. Zeqian Xu were involved in the contact angle measurements. Dr. Lutz Scheideler and Ms. Evi Kimmerle-Müller have provided the osteoblasts and guided the biological tests.

Parts of my thesis have been published in *Journal of Clinical Medicine*. Xingting Han, Neha Sharma, Zeqian Xu, Lutz Scheideler, Jürgen Geis-Gerstorfer, Frank Rupp, Florian M. Thieringer, Sebastian Spintzyk (2019) An In Vitro Study of Osteoblast Response on Fused-Filament Fabrication 3D Printed PEEK for Dental and Cranio-Maxillofacial Implants. *Journal of clinical medicine* 8(6), 771

For my thesis, I myself have carried out all the experiments and data analysis. I hereby declare that the thesis is my own unaided work. All direct or indirect sources used are acknowledged as references.

## **Acknowledgment**

I would like to express my most sincere gratitude to the following people or organizations:

First, I'd like to thank my academic supervisor, Prof. Dr. Jürgen Geis-Gerstorfer and Prof. Dr. Frank Rupp, for the help in this study and life during the past three years. With their support, I enrich my knowledge and enlarge my horizons.

Furthermore, Dr. Lutz Scheideler and Mr. Sebastian Spintzyk provide me a lot of support in the biological assessment and 3D-printing parts of this work, and they also made great suggestions for my doctoral thesis.

Dr. Florian M. Thieringer and Ms. Neha Sharma from the Department of Oral and Cranio-Maxillofacial Surgery, University Hospital Basel, Basel, Switzerland, are acknowledged for the FFF-printed PEEK samples preparation.

I would like to thank Ernst Schweizer for the assistance in the SEM analysis.

I acknowledge my sincere gratitude to my dear colleagues, Ms. Christine Schille, Ms. Ingrid Stephan, and Ms. Evi Kimmerle-Müller, who taught me a lot of the laboratory techniques.

The China Scholarship Council (CSC) is gratefully acknowledged for the financial support of Xingting Han (Grant 201606280045).

Finally, I'd like to thank my family for their support and encouragement throughout my study, especially my parents and my boyfriend.

## Curriculum Vitae

### Personal Information

Name: Xingting Han

Gender: Female

Date of birth: 21.08.1989

Nationality: Chinese

### Education

- |                     |   |
|---------------------|---|
| 09. 2005 – 06. 2008 | Xi'an Middle School, Xi'an, China   |
| 09. 2008 – 06. 2013 | Stomatological Medicine Faculty, Xi'an Jiaotong University, Xi'an, China. Bachelor Degree                                 |
| 09. 2013 – 06. 2016 | Stomatology, Stomatological Hospital of Xi'an Jiaotong University, Xi'an, China. Master Degree                            |
| since 10. 2016      | Department of Prosthodontics and Section "Medical Materials and Technology", University Hospital Tuebingen. Doctor Degree |

### Science Activities and Scholarships

- X. Han, T. Sawada, R. Ebert, M. Kaiser, J. Geis-Gerstorfer, S. Spintzyk (2017). Manufacturing process influence on Co–Cr base-alloy mechanical properties. *Dental Materials*, 33, e37-e38.
- Xingting Han, Tomofumi Sawada, Christine Schille, Ernst Schweizer, Lutz Scheideler, Jürgen Geis-Gerstorfer, Sebastian Spintzyk (2018). Comparative Analysis of Mechanical Properties and Metal-Ceramic Bond Strength of Co-Cr Dental Alloy Fabricated by Different Manufacturing Processes. *Materials*, 11(10), 1801.
- Xingting Han, Dong Yang, Chuncheng Yang, Sebastian Spintzyk, Lutz Scheideler, Ping Li, Dichen Li, Jürgen Geis-Gerstorfer, Frank Rupp (2019). Carbon Fiber Reinforced PEEK Composites Based on 3D-Printing Technology for Orthopedic and Dental Applications. *Journal of clinical medicine*, 8(2), 240.

- Xingting Han, Neha Sharma, Zeqian Xu, Lutz Scheideler, Jürgen Geis-Gerstorfer, Frank Rupp, Florian M. Thieringer, Sebastian Spintzyk (2019) An In Vitro Study of Osteoblast Response on Fused-Filament Fabrication 3D Printed PEEK for Dental and Cranio-Maxillofacial Implants. *Journal of clinical medicine* 8(6), 771.
- Scholarship from the Chinese Scholarship Council, 2016 – 2019.